Article

Factors Governing the Substitution of La for Ca and Mg in Metalloproteins: A DFT/CDM Study

Todor Dudev, Li-Ying Chang, and Carmay Lim

J. Am. Chem. Soc., **2005**, 127 (11), 4091-4103• DOI: 10.1021/ja044404t • Publication Date (Web): 24 February 2005

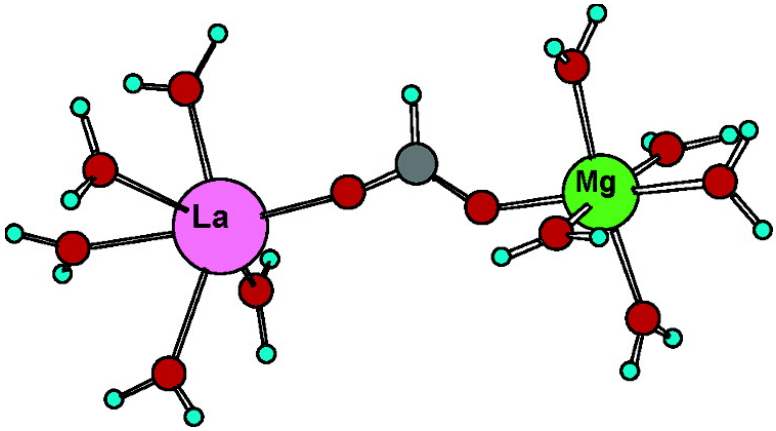

More About This Article

Additional resources and features associated with this article are available within the HTML version:

- Supporting Information
- Links to the 8 articles that cite this article, as of the time of this article download
- Access to high resolution figures
- Links to articles and content related to this article
- Copyright permission to reproduce figures and/or text from this article

View the Full Text HTML

J|A|C|S
ARTICLES
Published on Web 02/24/2005

Factors Governing the Substitution of La^{3+} for Ca^{2+} and Mg^{2+} in Metalloproteins: A DFT/CDM Study

Todor Dudev,[†] Li-Ying Chang,[‡] and Carmay Lim*,[†,‡]

Contribution from the Institute of Biomedical Sciences, Academia Sinica, Taipei 115, and Department of Chemistry, National Tsing Hua University, Hsinchu 300, Taiwan R.O.C.

Received September 15, 2004; E-mail: carmay@gate.sinica.edu.tw

Abstract: Trivalent lanthanide cations are extensively being used in biochemical experiments to probe various dication-binding sites in proteins; however, the factors governing the binding specificity of lanthanide cations for these binding sites remain unclear. Hence, we have performed systematic studies to evaluate the interactions between La^{3+} and model Ca^{2+}- and Mg^{2+}-binding sites using density functional theory combined with continuum dielectric methods. The calculations reveal the key factors and corresponding physical bases favoring the substitution of trivalent lanthanides for divalent Ca^{2+} and Mg^{2+} in holoproteins. Replacing Ca^{2+} or Mg^{2+} with La^{3+} is facilitated by (1) minimizing the solvent exposure and the flexibility of the metal-binding cavity, (2) freeing both carboxylate oxygen atoms of Asp/Glu side chains in the metal-binding site so that they could bind bidentately to La^{3+}, (3) *maximizing* the number of metal-bound carboxylate groups in *buried* sites, but *minimizing* the number of metal-bound carboxylate groups in *solvent-exposed* sites, and (4) including an Asn/Gln side chain for sites lined with four Asp/Glu side chains. In proteins bound to both Mg^{2+} and Ca^{2+}, La^{3+} would prefer to replace Ca^{2+}, as compared to Mg^{2+}. A second Mg^{2+}-binding site with a net positive charge would hamper the $Mg^{2+} \rightarrow La^{3+}$ exchange, as compared to the respective *mono*nuclear site, although the La^{3+} substitution of the first native metal is more favorable than the second one. The findings of this work are in accord with available experimental data.

Introduction

Lanthanide cations (Ln^{3+}) are increasingly being used in both crystallographic and spectroscopic studies of biological systems. The crystallographic applications involve using lanthanide ions to determine the phases of the diffracted X-rays by multiple isomorphous replacement or multiwavelength anomalous dispersion.[1,2] Spectroscopic applications include using luminescent lanthanide ions in bioanalytical assays[3,4] to determine the interdomain distance of proteins.[5] In particular, NMR spectroscopic applications make use of the large anisotropic magnetic susceptibility of paramagnetic lanthanides, which gives rise to large pseudocontact shifts that can be observed for residues as far as 40 Å from the metal center, to obtain long-distance restraints for protein structure determination.[6−9] However, to the best of our knowledge, no systematic theoretical studies have been performed to elucidate the factors governing the binding affinity and specificity of lanthanide cations for protein binding sites. To complement the experimental studies, we attempt here to provide some guidelines and physical principles governing the metal substitution (in particular Mg^{2+} and Ca^{2+}) by lanthanide cations.

Lanthanides have been extensively used to probe alkaline earth metal-binding sites (Ca^{2+}-binding sites in particular) in proteins, which have few chemical properties that can be used to explore their biochemistry in situ. Ln^{3+} shares certain physical and chemical properties with Mg^{2+} and Ca^{2+}.[10] Lanthanides, Mg^{2+}, and Ca^{2+} behave as hard-acid cations, preferring to bind "hard" bases containing oxygen and fluorine, rather than "soft" bases containing nitrogen, phosphorus, and sulfur.[11] Lanthanides also behave more like alkaline earth metal dications than like the transition metals in that their bonding is essentially ionic.[10] Directed "covalent" bonding typically observed in the transition elements is not seen in Ln^{3+} mainly because the f-electrons do not play a major role in lanthanide−ligand bonding.[12,13] A slight amount of covalency in lanthanide bonds has been attributed to the involvement of the lanthanide 6s orbitals rather than the 4f orbitals.[14] Lanthanides, exhibiting a range of ionic radii encompassing that of Ca^{2+}, appear to be almost ideal biomimetic

[†] Academia Sinica.
[‡] National Tsing Hua University.

(1) Matthews, B. W.; Weaver, L. H. *Biochemistry* **1974**, *13*, 1719−1725.
(2) Weis, W. I.; Kahn, R.; Fourme, R.; Drickamer, K.; Hendrickson, W. A. *Science* **1991**, *254*, 1608−1615.
(3) Horrocks, W. D., Jr. *Methods Enzymol.* **1993**, *226*, 495−538.
(4) Sabbatini, N.; Guardigli, M.; Lehn, J.-M. *Coord. Chem. Rev.* **1993**, *123*, 201−228.
(5) Dong, W.-J.; Robinson, J. M.; Xing, J.; Umeda, P. K.; Cheung, H. C. *Protein Sci.* **2000**, *9*, 280−289.
(6) Bentrop, D.; Bertini, I.; Cremonini, M. A.; Forsen, S.; Luchinat, C.; Malmendal, A. *Biochemistry* **1997**, *36*, 11605−11618.
(7) Barbieri, R.; Bertini, I.; Cavallaro, G.; Lee, Y.-M.; Luchinat, C.; Rosato, A. *J. Am. Chem. Soc.* **2000**, *124*, 5581−5587.
(8) Allegrozzi, M.; Bertini, I.; Janik, M. B. L.; Lee, Y.-M.; Liu, G.; Luchinat, C. *J. Am. Chem. Soc.* **2000**, *122*, 4154−4161.
(9) Bertini, I.; Janik, M. B.; Lee, Y. M.; Luchinat, C.; Rosato, A. *J. Am. Chem. Soc.* **2001**, *123*, 4181−4188.
(10) Evans, C. H. *Biochemistry of the Lanthanides*; Plenum: New York, 1990.
(11) Cotton, F. A.; Wilkinson, G. *Advanced Inorganic Chemisry*; Wiley & Sons: New York, 1988.
(12) *Handbook on the physics and chemistry of rare earths*; Gschneidner, K. A., Jr., Eyring, L., Eds.; North-Holland: Amsterdam, 1991; Vol. 15.
(13) Maron, L.; Eisenstein, O. *J. Phys. Chem. A* **2000**, *104*, 7140−7143.

10.1021/ja044404t CCC: $30.25

agents for Ca^{2+}. For example, lanthanum (La^{3+}) and Ca^{2+} have similar ionic radii: 1.17 and 1.14 Å, respectively, for six-coordinated ions, and 1.30 and 1.26 Å, respectively, for eight-coordinated ions.[15] Although Ln^{3+} has larger ionic radii than Mg^{2+} (0.86 Å[15] for six-coordinated Mg^{2+}), it has been successfully used to probe Mg^{2+}-binding sites as well.[16−23]

However, lanthanides also possess properties distinct from Mg^{2+} and Ca^{2+}. For example, La^{3+} is a better Lewis acid than Mg^{2+} and Ca^{2+} because the pK_a of the aqua ions is 11.4 for Mg^{2+} and 12.8 for Ca^{2+}, but 9.0 for La^{3+}.[24] The coordination chemistry of lanthanides appears to be more flexible than that of Mg^{2+} and Ca^{2+}.[25] A survey of lanthanide-binding sites composed of only amino acids and water molecules in the Protein Data Bank (PDB)[26] shows that the maximum coordination number (CN) is eight, while the average CN in Ca^{2+}-replaced binding sites is 7.2, whereas that in adventitious sites is 4.4.[27] On the other hand, the observed CN of Ca^{2+} in proteins varies from 6 to 9;[28] the average CN is six, while for EF-hand sites it is seven.[27] Unlike lanthanides and Ca^{2+}, the CN of Mg^{2+} in proteins is predominantly six.[29]

Partly because of the aforementioned properties of the lanthanide metals as well as their optical and paramagnetic properties, they have been widely used to replace Ca^{2+}, especially in EF-hand proteins, which are involved in many physiological processes such as muscle contraction, vision, cell cycle regulation, brain cortex and cerebellum modulation, and microtubule organization.[30] EF-hand proteins contain a Ca-binding motif (the EF-hand motif),[31] which has more than 500 entries in the PDB.[32] The canonical EF-hand motif consists of a contiguous 12-residue Ca-binding loop flanked by two helices forming a conserved helix−loop−helix structure.[33−35] Residues 1, 3, 5, 7, 9, and 12 of the Ca-binding loop bind Ca^{2+} in a pentagonal bipyramidal geometry.[36] Asp/Glu carboxylate side chains at loop positions 1, 3, and 5 coordinate monodentately to Ca^{2+}, whereas both Glu carboxylate oxygen atoms at the last loop position bind bidentately to Ca^{2+}. A backbone carbonyl oxygen of loop residue 7 and a water molecule bridging to loop residue 9 complete the heptacoordination geometry.[37,38] Out of these Ca^{2+}-binding residues, the monodentately bound aspartate, the backbone carbonyl group, the water molecule, and the bidentately bound glutamate at loop positions 1, 7, 9, and 12, respectively, are highly conserved.[39]

Lanthanides have also been used to probe Mg^{2+}-binding sites in enzymes, but to a more limited extent than Ca^{2+}-binding sites. Examples include a mononuclear binding site in malic enzymes[23] and binuclear binding sites in inositol monophosphatase[18,19,21] and some polymerases.[20,22] These metal-binding sites consist of two to three Asp or Glu residues, complemented, in some cases, by a backbone carbonyl group.[19,21,22]

Although Ca^{2+} and Mg^{2+} can be functionally replaced by various trivalent lanthanide ions,[3,10,16−23] many questions remain concerning the molecular aspects of this substitution. For example, (1) do the solvent exposure and the flexibility of the metal-binding site in the metal-bound protein (holoprotein) affect the $Ca^{2+}/Mg^{2+} \rightarrow Ln^{3+}$ substitution, and if so, to what extent? (2) Considering that the denticity of a ligand is known to play an important role in protein function[40] and in determining binding affinities and coordination geometries in small complexes,[27,41] how would the carboxylate-binding mode (monodentate/bidentate) affect the substitution of Ca^{2+} or Mg^{2+} for lanthanide ions? (3) What amino acid composition of Mg^{2+}- and Ca^{2+}-binding sites would favor the $Ca^{2+}/Mg^{2+} \rightarrow Ln^{3+}$ substitution? (4) In proteins where both Mg^{2+}- and Ca^{2+}-binding sites are present, which metal-binding site (Ca^{2+}/Mg^{2+}) would be more susceptible to Ln^{3+} substitution? (5) In proteins containing both mononuclear and binuclear metal-binding sites, which metal-binding site (mononuclear or binuclear) would be more susceptible to Ln^{3+} substitution and how would the Ln^{3+} substitution of the first native metal affect the thermodynamics of the second metal exchange?

To address the above questions, we have carried out systematic theoretical studies to evaluate the interactions between lanthanide cations and model Ca^{2+} and Mg^{2+} complexes. We chose to study La^{3+} among the lanthanides series for two reasons. First, La^{3+} is a closed-shell ion that will yield more reliable results from quantum chemical calculations (see below) than open-shell lanthanide ions. Second, its chemical properties are similar to those of the other lanthanides. To determine the most preferable Ca^{2+}/Mg^{2+}-binding site for La^{3+} to replace Ca^{2+}/Mg^{2+}, we computed the free energies for replacing Ca^{2+}/Mg^{2+} with La^{3+} in typical Ca^{2+}- and Mg^{2+}-binding sites containing different combinations of carboxylates and backbone amides using density functional theory (DFT) combined with continuum dielectric methods (CDM), as described in the next section. To assess if the solvent exposure and the flexibility of the metal-binding site in the holoprotein

(14) Gschneidner, K. A., Jr.; Eyring, L.; Choppin, G. R.; Lander, G. H. In *Handbook on the physics and chemistry of rare earths*; Gschneidner, K. A., Jr., Eyring, L., Eds.; North-Holland: Amsterdam, 1994; Vol. 18.
(15) Shannon, R. D. *Acta Crystallogr., Sect. A* **1976**, *32*, 751−767.
(16) McNemar, L. S. Ph.D. Thesis, The Pennsylvania State University, PA, 1989.
(17) Cornwall, E. Ph.D. Thesis, The Pennsylvania State University, PA, 1993.
(18) Bone, R.; Frank, L.; Springer, J. P.; Pollack, S. J.; Osborne, S.-A.; Atack, J. R.; Knowles, M. R.; McAllister, G.; Ragan, C. I.; Broughton, H. B.; Baker, R.; Fletcher, S. R. *Biochemistry* **1994**, *33*, 9460−9467.
(19) Bone, R.; Frank, L.; Springer, J. P.; Atack, J. R. *Biochemistry* **1994**, *33*, 9468−9476.
(20) Frey, M. W.; Frey, S. T.; Horrocks, W. D., Jr.; Kaboord, B. F.; Benkovic, S. J. *Chem. Biol.* **1996**, *3*, 393−403.
(21) Thorne, M. R.; Greasley, P. J.; Gore, M. G. *Biochem. J.* **1996**, *315*, 989−994.
(22) Brautigam, C. A.; Aschheim, K.; Steitz, T. A. *Chem. Biol.* **1999**, *6*, 901−908.
(23) Yang, Z.; Batra, R.; Floyd, D. L.; Hung, H.-C.; Chang, G.-G.; Tong, L. *Biochem. Biophys. Res. Commun.* **2000**, *274*, 440−444.
(24) Dean, J. A. In *Lange's Handbook of Chemistry*; Dean, J. A., Ed.; McGraw-Hill: New York, 1985.
(25) Martell, A. E.; Hancock, R. D. *Metal Complexes in Aqueous Solutions*; Plenum: New York, 1996.
(26) Abola, E. E.; Sussman, J. L.; Prilusky, J.; Manning, N. O. *Protein Data Bank Archives of Three-Dimensional Macromolecular Structures*; Academic Press: San Diego, CA, 1997; Vol. 277.
(27) Pidcock, E.; Moore, G. R. *J. Biol. Inorg. Chem.* **2001**, *6*, 479−489.
(28) Yang, W.; Jones, L. M.; Isley, L.; Ye, Y.; Lee, H.-W.; Wilkins, A.; Liu, Z.-r.; Hellinga, H. W.; Malchow, R.; Ghazi, M.; Yang, J. J. *J. Am. Chem. Soc.* **2003**, *125*, 6165−6171.
(29) Jernigan, R.; Raghunathan, G.; Bahar, I. *Curr. Opin. Struct. Biol.* **1994**, *4*, 256−263.
(30) Cates, M. S.; Berry, M. B.; Ho, E. L.; Li, Q.; Potter, J. D.; Phillips, G. N. *Structure* **1999**, *7*, 1269−1278.
(31) Lewit-Bentley, A.; Re'ty, S. *Curr. Opin. Struct. Biol.* **2000**, *10*, 637−643.
(32) Kawasaki, H.; Kretsinger, R. *Protein Profile* **1995**, *2*, 297−490.
(33) Krestinger, R. H.; Kockolds, C. E. *J. Biol. Chem.* **1973**, *248*, 3313−3326.
(34) Declercq, J.-P.; Tinant, B.; Parello, J.; Rambaud, J. *J. Mol. Biol.* **1991**, *220*, 1017−1039.
(35) Houdusse, A.; Cohen, C. *Structure* **1996**, *4*, 21−32.
(36) Strynadka, N. C.; James, M. N. *Annu. Rev. Biochem.* **1989**, *58*, 951−998.
(37) Falke, J. J.; Drake, S. K.; Hazard, A. L.; Peersen, O. B. *Q. Rev. Biophys.* **1994**, *27*, 219−290.
(38) Gopal, B.; Swaminathan, C. P.; Bhattacharya, S.; Bhattacharya, A.; Murthy, M. R. N.; Surolia, A. *Biochemistry* **1997**, *36*, 10910−10916.
(39) Yang, W.; Lee, H.-W.; Hellinga, H.; Yang, J. J. *Proteins: Struct., Funct., Genet.* **2002**, *47*, 344−356.
(40) Dudev, T.; Lim, C. *J. Phys. Chem. B* **2004**, *108*, 4546−4557.
(41) Ozawa, T.; Fukuda, M.; Nara, M.; Nakamura, A.; Komine, Y.; Kohama, K.; Umezawa, Y. *Biochemistry* **2000**, *39*, 14495−14503.

affect the $Ca^{2+}/Mg^{2+} \rightarrow Ln^{3+}$ exchange, we investigated mononuclear Mg^{2+}/Ca^{2+}-binding sites of varying degrees of solvent exposure that were either (i) rigid, forcing the incoming La^{3+} to adopt the native metal's coordination geometry or (ii) flexible, allowing the incoming La^{3+} to adopt its most favorable coordination configuration.[42] To evaluate the effect of the carboxylate-binding mode (monodentate/bidentate) on the $Ca^{2+} \rightarrow La^{3+}$ exchange, we examined classical EF-hand binding sites with and without changing the original carboxylate-binding mode. To determine the effect of the Ln^{3+} substitution of the first native metal on the thermodynamics of the second metal exchange, we examined $Mg^{2+} \rightarrow La^{3+}$ substitution reactions in model binuclear-binding sites. These calculations reveal the key factors and corresponding physical bases favoring $Ca^{2+}/Mg^{2+} \rightarrow Ln^{3+}$ substitution in Ca^{2+}/Mg^{2+} proteins.

Methods

Models Used. The metal and ligands forming the first shell were treated quantum mechanically to account for electronic effects such as charge transfer from the ligands to the metal. The rest of the protein was treated as a dielectric continuum characterized by various dielectric constants mimicking varying degrees of solvent exposure of the metal-binding site. The side chains of Asp and Glu, which are most commonly found bound to Ca^{2+}, Mg^{2+}, and lanthanides in proteins,[27,40,43] were modeled by formate, $HCOO^-$, while the side chains of Asn and Gln and the peptide backbone group were modeled by $HCONH_2$. Since Ca^{2+} is usually seven-coordinated in EF-hand proteins while Mg^{2+} is predominantly six-coordinated in proteins, the Ca^{2+} and Mg^{2+} complexes were modeled as Ca L_7 and Mg L_6, respectively (L = H_2O, $HCONH_2$, or $HCOO^-$). Lanthanum complexes were modeled as La L_6, La L_7, and La L_8. In *aqueous* solution, the CN of La^{3+} and Mg^{2+} have been measured to be nine and six,[44−46] respectively, while that of Ca^{2+} ranges between six and 10 with six appearing to be the most common.[45,47] Hence, Ca^{2+}, Mg^{2+}, and La^{3+} in aqueous solution were modeled as $[Ca(H_2O)_6]^{2+}$, $[Mg(H_2O)_6]^{2+}$, and $[La(H_2O)_9]^{3+}$ hydrates, respectively.

DFT Calculations. Full geometry optimization for each complex studied was carried out using the Gaussian 03 program[48] employing the S-VWN functional with the SDD effective core potential for La^{3+} and the 6-31+G* basis set for all the other atoms. This functional/basis set combination was chosen as it reproduces the experimentally observed metal−O bond distances in La^{3+}, Ca^{2+}, and Mg^{2+} hydrates within the experimental error (Table 1).

For each fully optimized structure, S-VWN/(SDD, 6-31+G*) vibrational frequencies were computed to verify that the molecule was at the minimum of its potential energy surface. No imaginary frequency was found in any of the metal complexes. After scaling the frequencies by an empirical factor of 0.9833,[49] we evaluated the thermal energy including zero point energy (E_T), work (PV) and entropy (S) corrections using standard statistical mechanical formulas.[50] The electronic energies E_{elec} were then evaluated at the B3-LYP/(SDD, 6-31+G*)//S-VWN/(SDD, 6-31+G*) level. The differences ΔE_{elec}, ΔE_T, ΔPV, and ΔS between the products and reactants were used to compute the reaction free energy at room temperature, $T = 298.15$ K, according to the following expression:

$$\Delta G^1 = \Delta E_{elec} + \Delta E_T + \Delta PV - T\Delta S \quad (1)$$

Table 1. Comparison between Computed and Experimental Average Metal−O Distances in $[La(H_2O)_9]^{3+}$, $[Ca(H_2O)_6]^{2+}$, and $[Mg(H_2O)_6]^{2+}$

	Metal–O (Å)	
molecule[a]	calcd[b]	expt[c]
$[La(H_2O)_9]^{3+}$	2.55	2.55 ± 0.04
$[Ca(H_2O)_6]^{2+}$	2.36	2.34 ± 0.07
$[Mg(H_2O)_6]^{2+}$	2.05	2.07 ± 0.03

[a] The CN of La^{3+} and Mg^{2+} in aqueous solution are nine[45] and six,[44,51] respectively, while that of Ca^{2+} ranges between six and 10, with six appearing to be the most common.[45,47] [b] From fully optimized S-VWN/(SDD, 6-31+G*) geometries. [c] From Cambridge Structure Database analysis; this work.

Scheme 1

$$\begin{array}{ccc} & \xrightarrow{\Delta G^1} & \\ \text{Reactants } (\varepsilon = 1) & \rightarrow & \text{Products } (\varepsilon = 1) \\ \Delta G_{solv}^{\ x}(\text{Reactants}) \downarrow & & \downarrow \Delta G_{solv}^{\ x}(\text{Products}) \\ \text{Reactants } (\varepsilon = x) & \rightarrow & \text{Products } (\varepsilon = x) \\ & \xrightarrow{\Delta G^x} & \end{array}$$

Continuum Dielectric Calculations. The reaction free energy in a given environment characterized by a dielectric constant $\epsilon = x$ can be calculated according to Scheme 1. ΔG^1 is the gas-phase free energy computed using eq 1, as described above. $\Delta G_{solv}^{\ x}$ is the free energy for transferring a molecule in the gas phase to a continuous solvent medium characterized by a dielectric constant, x. By solving Poisson's equation using finite difference methods[52,53] to estimate $\Delta G_{solv}^{\ x}$ (see below), the reaction free energy in an environment modeled by dielectric constant x, ΔG^x, can be computed from:

$$\Delta G^x = \Delta G^1 + \Delta G_{solv}^{\ x}(\text{products}) - \Delta G_{solv}^{\ x}(\text{reactants}) \quad (2)$$

The continuum dielectric calculations employed a 71 × 71 × 71 lattice with an initial grid spacing of 1.0 Å and were refined with a spacing of 0.25 Å, ab initio geometries, and natural bond orbital (NBO) atomic charges.[54] The low dielectric region of the solute was defined as the region inaccessible to contact by a 1.4 Å radius sphere rolling over the molecular surface. This region was assigned a dielectric constant of two ($\epsilon_{in} = 2$) to account for the electronic polarizability of the solute. The molecular surface was defined by *effective* solute radii, which were obtained by adjusting the CHARMM (version 22)[55] van

(42) Dudev, T.; Lim, C. *J. Phys. Chem. B* **2001**, *105*, 4446−4452.
(43) Dudev, T.; Cowan, J. A.; Lim, C. *J. Am. Chem. Soc.* **1999**, *121*, 7665−7673.
(44) Marcus, Y. *Chem. Rev.* **1988**, *88*, 1475−1498.
(45) Ohtaki, H.; Radnai, T. *Chem. Rev.* **1993**, *93*, 1157−1204.
(46) Markham, G. D.; Glusker, J. P.; Bock, C. L.; Trachtman, M.; Bock, C. W. *J. Am. Chem. Soc.* **1996**, *100*, 3488−3497.
(47) Harding, M. M. *Acta Crystallogr.* **1999**, *D55*, 1432−1443.
(48) Frisch, M. J.; Trucks, G. W.; Schlegel, H. B.; Scuseria, G. E.; Robb, M. A.; Cheeseman, J. R.; Montgomery, J. A., Jr.; Vreven, T.; Kudin, K. N.; Burant, J. C.; Millam, J. M.; Iyengar, S. S.; Tomasi, J.; Barone, V.; Mennucci, B.; Cossi, M.; Scalmani, G.; Rega, N.; Petersson, G. A.; Nakatsuji, H.; Hada, M.; Ehara, M.; Toyota, K.; Fukuda, R.; Hasegawa, J.; Ishida, M.; Nakajima, T.; Honda, Y.; Kitao, O.; Nakai, H.; Klene, M.; Li, X.; Knox, J. E.; Hratchian, H. P.; Cross, J. B.; Adamo, C.; Jaramillo, J.; Gomperts, R.; Stratmann, R. E.; Yazyev, O.; Austin, A. J.; Cammi, R.; Pomelli, C.; Ochterski, J. W.; Ayala, P. Y.; Morokuma, K.; Voth, G. A.; Salvador, P.; Dannenberg, J. J.; Zakrzewski, V. G.; Dapprich, S.; Daniels, A. D.; Strain, M. C.; Farkas, O.; Malick, D. K.; Rabuck, A. D.; Raghavachari, K.; Foresman, J. B.; Ortiz, J. V.; Cui, Q.; Baboul, A. G.; Clifford, S.; Cioslowski, J.; Stefanov, B. B.; Liu, G.; Liashenko, A.; Piskorz, P.; Komaromi, I.; Martin, R. L.; Fox, D. J.; Keith, T.; Al-Laham, M. A.; Peng, C. Y.; Nanayakkara, A.; Challacombe, M.; Gill, P. M. W.; Johnson, B.; Chen, W.; Wong, M. W.; Gonzalez, C.; Pople, J. A. *Gaussian 03*, revision B.01; Gaussian, Inc.: Pittsburgh, PA, 2003.
(49) Wong, M. W. *Chem. Phys. Lett.* **1996**, *256*, 391−399.
(50) McQuarrie, D. A. *Statistical Mechanics*; Harper and Row: New York, 1976.
(51) Markham, G. D.; Glusker, J. P.; Bock, C. W. *J. Phys. Chem. B* **2002**, *106*, 5118−5134.
(52) Gilson, M. K.; Honig, B. *Biopolymers* **1986**, *25*, 2097−2119.
(53) Lim, C.; Bashford, D.; Karplus, M. *J. Phys. Chem.* **1991**, *95*, 5610−5620.
(54) Reed, A. E.; Curtiss, L. A.; Weinhold, F. *Chem. Rev.* **1988**, *88*, 899−926.
(55) Brooks, B. R.; Bruccoleri, R. E.; Olafson, B. D.; States, D. J.; Swaminathan, S.; Karplus, M. *J. Comput. Chem.* **1983**, *4*, 187−217.

Table 2. Comparison between Computed and Experimental Hydration Free Energies

	ΔG_{solv}^{80} (kcal/mol)		
metal/ligand	calcd	expt	error[a]
La^{3+}	−791.7	−791.1[b]	−0.6
Ca^{2+}	−381.5	−380.8[b]	−0.7
Mg^{2+}	−456.3	−455.5[b]	−0.8
$HCOO^-$	−82.1	−82.0[c]	−0.1
$HCONH_2$	−10.6	−10.0[d]	−0.6
H_2O	−7.1	−6.3[e]	−0.8

[a] Error = ΔG_{solv}^{80}(calcd) − ΔG_{solv}^{80}(expt). [b] From Friedman and Krishnan, 1973.[57] [c] From Lim et al., 1991.[53] [d] Experimental solvation free energy of HCONH(CH_3) from Wolfenden, 1978.[58] [e] From Ben-Naim and Marcus, 1984.[59]

der Waals radii to reproduce the experimental hydration free energies of the metal cations and ligands (see below and Table 2). Poisson's equation was solved with $\epsilon_{in} = 2$ and $\epsilon_{out} = 1$, 4, 10, 20, or 80 to yield electrostatic potentials in the gas phase ($\epsilon_{out} = 1$) and in protein cavities with increasing solvent exposure (represented by increasing ϵ_{out}). The difference between the computed electrostatic potentials in a given dielectric medium ($\epsilon_{out} = x$) and in the gas phase ($\epsilon_{out} = 1$) yielded the solvation free energy ΔG_{solv}^{x}.

The effective solute radii, which have been parametrized for S-VWN/(SDD, 6-31+G*) geometries and NBO charges, are as follows (in Å): $R_{La} = 2.15$, $R_{Ca} = 1.75$, $R_{Mg} = 1.50$, $R_{C,sp2} = 1.88$, $R_N = 1.75$, $R_O(H_2O) = 1.84$, $R_O(HCONH_2) = 1.78$, $R_O(H_2O-Metal) = 1.70$, $R_O(HCOO^-) = 1.60$, $R_H = 1.468$, $R_H(H_2O-La) = 0.98$, $R_H(H_2O-Ca) = 1.09$, and $R_H(H_2O-Mg) = 1.16$. These effective solute radii consistently overestimate the magnitude of the experimental hydration free energies of the metal cations and individual ligands by less than 1 kcal/mol (see Table 2). Note that by adjusting the solute radii to reproduce *experimental* hydration free energies, errors in computing ΔG_{solv}^{80} due to (a) the assumption of the gas-phase geometry in the different dielectric environments, (b) uncertainties in the dielectric boundary, and (c) the neglect of nonelectrostatic solute−solvent interactions are implicitly taken into account.[56]

Results

In this work, we compute the free energies for replacing the native cofactor (Ca^{2+} or Mg^{2+}) with La^{3+} in various model metal-binding sites. In modeling the metal exchange reactions we assume the following steps: First, a hydrated La^{3+} from aqueous solution is able to find the metal-bound cavity. Next, the metal-exchange reaction (eqs 3−5) occurs in the metal-binding site, characterized by a given dielectric constant. Finally, the native metal cofactor (Ca^{2+} or Mg^{2+}) and water molecule(s) are released into solution. Because our interest is in how properties of the metal-binding site (such as its flexibility and number of metal-bound carboxylate or carbonyl oxygen atoms) affect the $Ca^{2+}/Mg^{2+} \rightarrow La^{3+}$ substitution, we focus on the free energy change between *two* reactions. Therefore, factors that are common for the two reactions such as the desolvation of La^{3+} in coming from aqueous solution to the metal cavity and the solvation of Ca^{2+}/Mg^{2+} and water molecules in leaving the cavity to solution would cancel.

La^{3+} as a Substitute for Ca^{2+}. Dependence on the Number of Carboxylate Groups. We first assessed how the number of formate molecules bound to Ca^{2+} affects the free energy for replacing Ca^{2+} with La^{3+} in model Ca-binding sites, consisting of Ca^{2+} heptacoordinated to a formate bidentately (denoted by HCÕÕ), one to three formates monodentately (denoted by HCOO), and water molecules (denoted by W) in the absence and presence of a formamide. Two cases were considered assuming that La^{3+} retains the same carboxylate-binding mode as Ca^{2+}. In the first case, metal exchange takes place in a rigid binding site (Table 3, reactions 1−8), where the holoprotein matrix does not allow any amino acid rearrangements upon La^{3+} substitution. Thus, La^{3+} adopts the same CN as Ca^{2+} of seven:

$$[Ca\ W_{5-m-n}(HCONH_2)_m\ (HC\tilde{O}\tilde{O})\ (HCOO)_n]^{1-n} + [La\ W_9]^{3+} \rightarrow [La\ W_{5-m-n}\ (HCONH_2)_m\ (HC\tilde{O}\tilde{O})\ (HCOO)_n]^{2-n} + [Ca\ W_6]^{2+} + 3H_2O \quad m = 0, 1; n = 0, 1, 2, 3 \quad (3a)$$

The second case differs from the first in that the metal exchange occurs in a flexible binding site in the holoprotein (Table 3, reactions 9−12) that allows La^{3+} to expand the CN from seven to eight.

$$[Ca\ W_{5-n}\ (HC\tilde{O}\tilde{O})\ (HCOO)_n]^{1-n} + [La\ W_9]^{3+} \rightarrow [La\ W_{6-n}\ (HC\tilde{O}\tilde{O})\ (HCOO)_n]^{2-n} + [Ca\ W_6]^{2+} + 2H_2O \quad n = 0, 1, 2, 3 \quad (3b)$$

The $Ca^{2+} \rightarrow La^{3+}$ exchange free energies, ΔG^x, for eqs 3a and 3b in metal-binding sites of various degrees of solvent exposure, modeled by dielectric constants, x, ranging from 4 to 80, were computed according to Scheme 1. For buried or partially buried ($4 < x < 80$) metal-binding sites, we need to also consider desolvation of $[La\ W_9]^{3+}$ and solvation of $[Ca\ W_6]^{2+}$ and the released water molecules. These effects, however, cancel in comparing two reactions with the same $[La\ W_9]^{3+}$ coming in from aqueous solution and the same products ($[Ca\ W_6]^{2+}$ and nH_2O) released into solution (see below).

Both heptacoordinated Ca^{2+} and La^{3+} structures adopt an irregular geometry without a clear preference for a particular symmetry (Figures 1 and 2). For both Ca^{2+} and La^{3+} complexes, monodentate carboxylates are stabilized by hydrogen bonds with neighboring water ligand(s), and their average metal−O bond length is shorter than the respective metal−Õ(bidentate) bond distance (by 0.07 to 0.09 Å). However, the average metal−O^{HCOO} (2.40 Å) and metal−Õ (2.47 Å) bond distances in Ca^{2+} complexes are shorter than those (2.43 and 2.52 Å) in the respective La^{3+} complexes (by 0.03 and 0. 05 Å).

Comparison of the $Ca^{2+} \rightarrow La^{3+}$ exchange free energies in going from reaction 1 → 4 in Table 3 reveals that whether increasing the number of carboxylates that can coordinate to La^{3+} could facilitate it to replace Ca^{2+} depends on the relative solvent exposure of the metal-binding site. In the gas phase and in buried Ca-binding sites, the $Ca^{2+} \rightarrow La^{3+}$ exchange in Ca−carboxylate complexes becomes *more* favorable with an increasing number of $HCOO^-$ bound to the metal (Table 3, ΔG^x values, $x \leq 10$, in going from reaction 1 → 4 become more negative), implying that the more $HCOO^-$ there are in the Ca^{2+} complex, the more thermodynamically favorable for La^{3+} to replace Ca^{2+}. This is partly because La^{3+} can accept more negative charge from the formates than Ca^{2+}, as evidenced by the greater charge transfer to La^{3+} compared to that for Ca^{2+}

(56) Dudev, T.; Lim, C. *J. Am. Chem. Soc.* **2000**, *122*, 11146−11153.
(57) Friedman, H. L.; Krishnan, C. V. *Thermodynamics of ionic hydration*; Plenum Press: New York, 1973; Vol. 3.
(58) Wolfenden, R. *Biochemistry* **1978**, *17*, 201−204.
(59) Ben-Naim, A.; Marcus, Y. *J. Chem. Phys.* **1984**, *81*, 2016−2027.

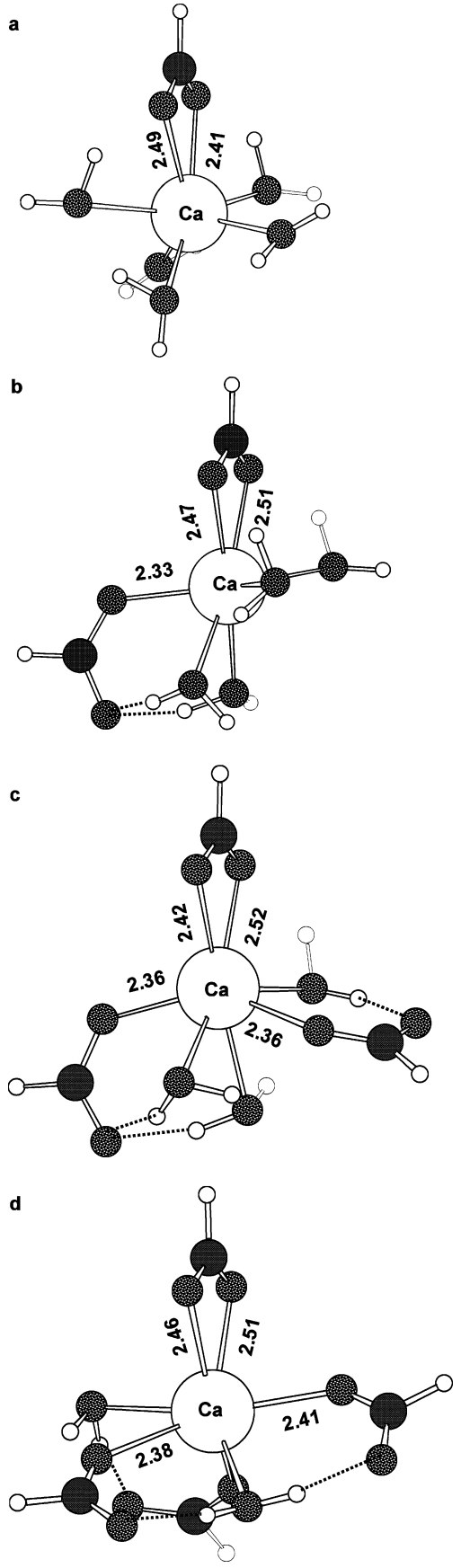

Figure 1. Ball-and-stick diagram of the fully optimized hepta-coordinated (a) $[Ca\ W_5\ (HC\tilde{O}\tilde{O})]^{+}$, (b) $[Ca\ W_4\ (HC\tilde{O}\tilde{O})\ (HCOO)]^{0}$, (c) $[Ca\ W_3\ (HC\tilde{O}\tilde{O})\ (HCOO)_2]^{-}$, and (d) $[Ca\ W_2\ (HC\tilde{O}\tilde{O})\ (HCOO)_3]^{-2}$.

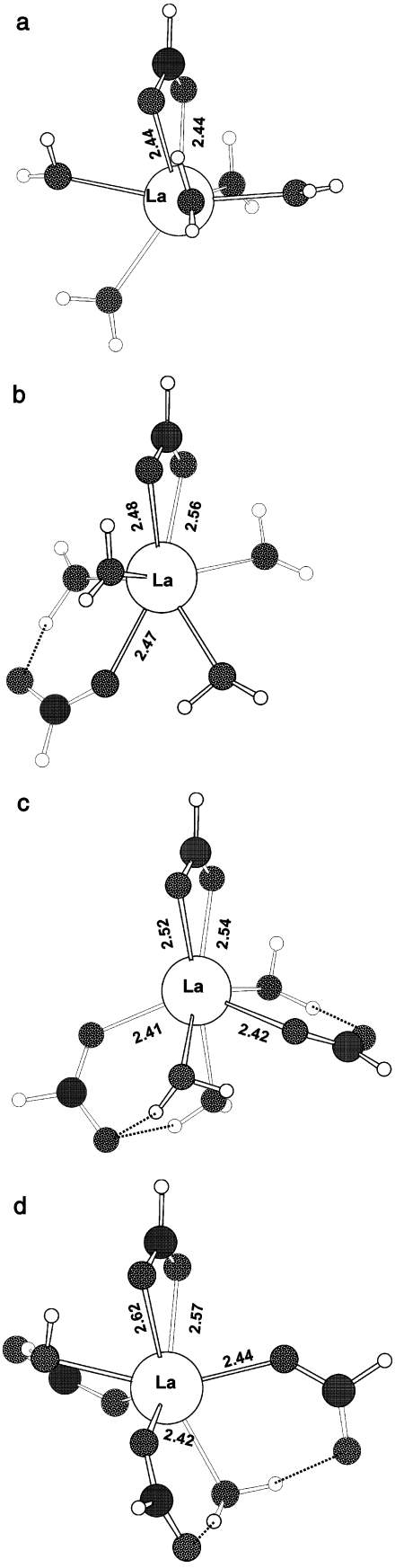

Figure 2. Ball-and-stick diagram of the fully optimized hepta-coordinated (a) $[La\ W_5\ (HC\tilde{O}\tilde{O})]^{2+}$, (b) $[La\ W_4\ (HC\tilde{O}\tilde{O})\ (HCOO)]^{+}$, (c) $[La\ W_3\ (HC\tilde{O}\tilde{O})\ (HCOO)_2]^{0}$, and (d) $[La\ W_2\ (HC\tilde{O}\tilde{O})\ (HCOO)_3]^{-}$.

Table 3. Calculated ΔG^x (kcal/mol) for $Ca^{2+} \rightarrow La^{3+}$ Exchange without Changing the Carboxylate Binding Mode in Seven-Coordinated Ca Complexes in Media of Dielectric Constant, *x*

reaction no.	reactant metal complex + $[La\,W_9]^{3+}$	product metal complex + $[Ca\,W_6]^{2+}$	$\Delta\Delta q^a$	$\Delta H^{1,b}$	$T\Delta S^{1,b}$	$\Delta G^{1,b}$	ΔG^4	ΔG^{10}	ΔG^{20}	$\Delta G^{80,c}$
	Rigid Sites, $CN^{Ca} = 7$; $CN^{La} = 7$	Same Formate Binding Mode								
1	$[Ca\,W_5(HC\tilde{O}\tilde{O})]^+$	$[LaW_5(HC\tilde{O}\tilde{O})]^{2+} + 3W$	0.19	−24.2	31.2	−55.4	−18.1	−12.1	−10.9	−7.2
2	$[Ca\,W_4(HC\tilde{O}\tilde{O})\,(HCOO)]^0$	$[LaW_4(HC\tilde{O}\tilde{O})\,(HCOO)]^+ + 3W$	0.16	−113.4	29.2	−142.6	−32.7	−11.1	−4.2	4.1
3	$[Ca\,W_3(HC\tilde{O}\tilde{O})\,(HCOO)_2]^-$	$[LaW_3(HC\tilde{O}\tilde{O})\,(HCOO)_2]^0 + 3W$	0.19	−192.4	28.8	−221.2	−47.7	−13.4	−2.2	9.3
4	$[Ca\,W_2(HC\tilde{O}\tilde{O})\,(HCOO)_3]^{-2}$	$[LaW_2(HC\tilde{O}\tilde{O})\,(HCOO)_3]^- + 3W$	0.19	−272.4	27.8	−300.2	−64.9	−16.7	−0.8	14.5
5	$[Ca\,W_4\,Fm\,(HC\tilde{O}\tilde{O})]^+$	$[La\,W_4\,Fm\,(HC\tilde{O}\tilde{O})]^{2+} + 3W$	0.19	−33.5	31.4	−64.9	−15.7	−7.0	−4.7	−0.1
6	$[Ca\,W_3\,Fm\,(HC\tilde{O}\tilde{O})\,(HCOO)]^0$	$[La\,W_3\,Fm\,(HC\tilde{O}\tilde{O})\,(HCOO)]^+ + 3W$	0.17	−117.1	30.7	−147.8	−33.1	−10.5	−3.6	5.3
7	$[Ca\,W_2\,Fm\,(HC\tilde{O}\tilde{O})\,(HCOO)_2]^-$	$[La\,W_2\,Fm\,(HC\tilde{O}\tilde{O})\,(HCOO)_2]^0 + 3W$	0.18	−196.5	29.0	−225.5	−49.2	−13.3	−1.5	10.8
8	$[Ca\,W_1\,Fm\,(HC\tilde{O}\tilde{O})\,(HCOO)_3]^{-2}$	$[La\,W_1\,Fm\,(HC\tilde{O}\tilde{O})\,(HCOO)_3]^- + 3W$	0.18	−276.2	27.7	−303.9	−69.7	−21.0	−4.5	11.3
	Flexible Sites, $CN^{Ca} = 7$; $CN^{La} = 8$	Same Formate Binding Mode								
9	$[Ca\,W_5(HC\tilde{O}\tilde{O})]^+$	$[LaW_6(HC\tilde{O}\tilde{O})]^{2+} + 2W$	0.19	−45.0	18.5	−63.5	−15.8	−6.8	−4.2	−0.1
10	$[Ca\,W_4(HC\tilde{O}\tilde{O})\,(HCOO)]^0$	$[LaW_5(HC\tilde{O}\tilde{O})\,(HCOO)]^+ + 2W$	0.19	−126.9	18.9	−145.8	−33.2	−10.8	−3.5	4.2
11	$[Ca\,W_3(HC\tilde{O}\tilde{O})\,(HCOO)_2]^-$	$[LaW_4(HC\tilde{O}\tilde{O})\,(HCOO)_2]^0 + 2W$	0.20	−203.5	17.1	−220.6	−42.2	−6.3	5.5	16.7
12	$[Ca\,W_2(HC\tilde{O}\tilde{O})\,(HCOO)_3]^{-2}$	$[LaW_3(HC\tilde{O}\tilde{O})\,(HCOO)_3]^- + 2W$	0.20	−284.2	16.2	−300.4	−60.3	−10.5	6.3	21.4

[a] $\Delta\Delta q = \Delta q_{La} - \Delta q_{Ca} = (3 - q_{La}) - (2 - q_{Ca})$. [b] Computed at the B3-LYP/(SDD, 6-31+G*)//S-VWN/(SDD, 6-31+G*) level. [c] Computed using the *experimental* hydration free energy of water (−6.3 kcal/mol[59]).

(Table 3, positive ΔΔq). On the other hand, in partially or fully solvent-exposed Ca-binding sites, the $Ca^{2+} \rightarrow La^{3+}$ exchange becomes *less* favorable with an increasing number of $HCOO^-$ bound to the metal (Table 3, ΔG^x values, $x \geq 20$, in going from reaction 1 → 4 become less negative and more positive), implying that the fewer $HCOO^-$ there are in the Ca^{2+} complex, the more thermodynamically favorable it is for La^{3+} to replace Ca^{2+}. This is largely because in monocarboxylate metal complexes, the dicationic La-substituted complex is better solvated than the monocationic native Ca complex, resulting in a solvation free energy gain, but as the number of carboxylates in the metal complex increases to four, the desolvation cost of a monoanionic or dianionic Ca complex outweighs the solvation free energy gain of the respective neutral or monoanionic La-substituted complex. In conclusion, increasing the number of carboxylates helps La^{3+} to replace Ca^{2+} in a *buried* metal-binding site, but *not* in a solvent-exposed site.

Dependence on a Neutral Carbonyl Group. Comparison of the $Ca^{2+} \rightarrow La^{3+}$ exchange free energies for reactions 5−8 with those for reactions 1−4, respectively, in Table 3 shows that whether including a carbonyl group that can coordinate to La^{3+} could help it to replace Ca^{2+} depends on the relative size of the Ca^{2+}−carboxylate complex. In the gas phase, the presence of a Ca-bound formamide facilitates the $Ca^{2+} \rightarrow La^{3+}$ exchange (Table 3, ΔG^1 values for reactions 5−8 are more negative than those for reactions 1−4, respectively). In condensed media, however, solvation effects are generally more unfavorable for the bulkier complexes with a formamide than those for the respective complexes without a formamide: in Table 3, the solvation free energy differences between products and reactants in buried sites, $\Delta\Delta G_{solv}{}^4$, are 49, 115, 176, and 234 kcal/mol in going from reaction 5 → 8, but are 37, 110, 174, and 235 kcal/mol, respectively, in going from reaction 1 → 4. Note that the $\Delta\Delta G_{solv}{}^x$, $x \geq 4$, difference between complexes with and without a formamide diminishes as more formates are bound to the metal and is similar when the metal is bound to four formates. Consequently, the presence of a Ca-bound formamide facilitates the $Ca^{2+} \rightarrow La^{3+}$ exchange only in the largest Ca^{2+} complex containing four carboxylates (Table 3, ΔG^x, $x < 80$, for reaction 8 is more negative than that for reaction 4). Including a carbonyl group in the metal's first shell, however, does not generally change the trends in the ΔG^x for $Ca^{2+} \rightarrow La^{3+}$ exchange as a function of the number of bound $HCOO^-$.

Dependence on the Metal CN. Comparison of the $Ca^{2+} \rightarrow La^{3+}$ exchange free energies for reactions 9−12 with those for reactions 1−4, respectively, in Table 3 shows that a flexible site in the holoprotein that allows La^{3+} to expand its CN from seven to eight does *not* facilitate La^{3+} to replace Ca^{2+} (Table 3, ΔG^x values, $x \geq 4$, for reactions 9−12 are generally less negative and more positive than those for reactions 1−4, respectively). Expanding the La^{3+} CN from seven to eight incurs a solute entropic loss (Table 3, ΔS^1 values for reactions 9−12 are less positive than those for reactions 1−4). Furthermore, the bigger *octa*coordinated La^{3+} complexes are generally not as well solvated as the respective *hepta*coordinated complexes. In addition, as compared to reactions 9−12, an extra water molecule is released upon metal exchange in a rigid site, and upon escaping from the metal-binding site into solution, it contributes an additional −3.0, −1.4, and −0.6 kcal/mol to ΔG^4, ΔG^{10}, and ΔG^{20} for reactions 1−4 in Table 3, respectively, making metal exchange in rigid sites even more favorable than that in flexible sites. Therefore, a rigid Ca-binding site would help La^{3+} to replace Ca^{2+} more than a flexible one.

As Ca^{2+} ion could adopt a CN other than six in aqueous solution, the *absolute* free energies (but not the *trend*) for eqs 3a and 3b will depend on its CN in the aqua complex and, hence, on the number of water molecules released upon $Ca^{2+} \rightarrow La^{3+}$ exchange. Increasing the Ca^{2+} CN in the aqua complex from six to seven or eight decreases the number of water molecules released upon metal substitution, leading to a less positive gas-phase entropy and a reduced solvation free energy gain of the freed water molecules. Moreover, $[Ca\,W_7]^{2+}$ and $[Ca\,W_8]^{2+}$ are bulkier than $[Ca\,W_6]^{2+}$ and are thus less well-solvated than the latter. These factors would result in a less negative ΔG^x for a hepta- or octahydrated Ca^{2+} as compared to that for a hexahydrated Ca^{2+}, but they would not change the trends noted above.

Dependence on the Carboxylate-Binding Mode. We next assessed how the carboxylate binding mode affects the $Ca^{2+} \rightarrow La^{3+}$ substitution in pseudo-classical EF-hand binding sites (without coordination to the peptide backbone, see Introduction), modeled by Ca heptacoordinated to a bidentate formate, three

Table 4. Calculated ΔG^x (kcal/mol) for $Ca^{2+} \rightarrow La^{3+}$ Exchange Accompanied by a Carboxylate-Binding Mode Change in Seven-Coordinated Ca Complexes in Media of Dielectric Constant, x

reaction No.	reactant metal complex + $[La\,W_9]^{3+}$	product metal complex + $[Ca\,W_6]^{2+}$	$\Delta\Delta q^a$	$\Delta H^{1,b}$	$T\Delta S^{1,b}$	$\Delta G^{1,b}$	ΔG^4	ΔG^{10}	ΔG^{20}	$\Delta G^{80,c}$
	Rigid Sites, $CN^{Ca} = CN^{La} = 7$	Different Formate Binding Mode								
1	$[Ca\,W_2(HC\tilde{O}\tilde{O})(HCOO)_3]^{-2}$	$[LaW_3(HCOO)_4]^- + 2W$	0.18	−276.5	16.9	−293.4	−56.6	−8.4	7.6	21.8
2	$[Ca\,W_2(HC\tilde{O}\tilde{O})(HCOO)_3]^{-2}$	$[LaW_2(HC\tilde{O}\tilde{O})(HCOO)_3]^- + 3W$	0.19	−272.4	27.8	−300.2	−64.9	−16.7	−0.8	14.5
3	$[Ca\,W_2(HC\tilde{O}\tilde{O})(HCOO)_3]^{-2}$	$[LaW(HC\tilde{O}\tilde{O})_2(HCOO)_2]^- + 4W$	0.21	−263.2	39.8	−303.0	−71.2	−24.0	−8.4	7.5
4	$[Ca\,W_2(HC\tilde{O}\tilde{O})(HCOO)_3]^{-2}$	$[La(HC\tilde{O}\tilde{O})_3(HCOO)]^- + 5W$	0.23	−243.1	52.2	−295.3	−70.5	−25.9	−11.6	4.1
	Flexible Sites, $CN^{Ca} = 7$; $CN^{La} = 8$	Different Formate Binding Mode								
5	$[Ca\,W_2(HC\tilde{O}\tilde{O})(HCOO)_3]^{-2}$	$[LaW_4(HCOO)_4]^- + W$	0.20	−289.0	4.4	−293.4	−50.5	0.5	17.9	32.6
6	$[Ca\,W_2(HC\tilde{O}\tilde{O})(HCOO)_3]^{-2}$	$[LaW_3(HC\tilde{O}\tilde{O})(HCOO)_3]^- + 2W$	0.20	−284.2	16.2	−300.4	−60.3	−10.5	6.3	21.4
7	$[Ca\,W_2(HC\tilde{O}\tilde{O})(HCOO)_3]^{-2}$	$[LaW_2(HC\tilde{O}\tilde{O})_2(HCOO)_2]^- + 3W$	0.22	−270.2	27.5	−297.7	−63.1	−15.0	1.0	16.4
8	$[Ca\,W_2(HC\tilde{O}\tilde{O})(HCOO)_3]^{-2}$	$[LaW(HC\tilde{O}\tilde{O})_3(HCOO)]^- + 4W$	0.23	−259.4	39.7	−299.1	−67.9	−20.9	−5.4	10.6
9	$[Ca\,W_2(HC\tilde{O}\tilde{O})(HCOO)_3]^{-2}$	$[La(HC\tilde{O}\tilde{O})_4]^- + 5W$	0.25	−246.2	50.6	−296.8	−71.8	−26.7	−12.1	4.1

[a] $\Delta\Delta q = \Delta q_{La} - \Delta q_{Ca} = (3 - q_{La}) - (2 - q_{Ca})$. [b] Computed at the B3-LYP/(SDD, 6-31+G*)//S-VWN/(SDD, 6-31+G*) level. [c] Computed using the *experimental* hydration free energy of water (−6.3 kcal/mol[59]).

monodentate formates, and two water molecules (Figure 1d). We considered the four formates binding in various combinations of monodentate and bidentate modes to either a *hepta*coordinated La^{3+} (Table 4, reactions 1−4) or an *octa*coordinated La^{3+} (Table 4, reactions 5−9).

The results in Table 4 show that La^{3+} prefers to bind to the carboxylates bidentately rather than monodentately, irrespective of the solvent exposure of the metal-binding site. In the gas phase, the ΔG^1 values for reactions 2−4 or reactions 6−9 with one or more formates bidentately bound are more negative than the ΔG^1 values for reactions 1 and 5, respectively, with *no* formates bidentately bound. This appears to be a consequence of favorable entropic effects accompanying the release of metal-bound water molecules upon binding the formates bidentately: the ΔS^1 term becomes more favorable (more positive), whereas the ΔH^1 term becomes less favorable (less negative) with an increasing number of formates bound bidentately to La^{3+} (Table 4). Because of the opposite contributions from the enthalpic and entropic terms to the gas-phase free energy, the most negative ΔG^1 corresponds to La^{3+} *hepta*coordinated to a water molecule, two bidentate formates, and two monodentate formates (Table 4, $\Delta G^1 = -303$ kcal/mol for reaction 3). On the other hand, the condensed-phase ΔG^x values, $x \geq 4$, become more favorable (more negative and less positive) with an increasing number of carboxylates bound *bidentately* to La^{3+} because the release of water molecules in the metal-binding site upon monodentate → bidentate formate binding results in a solvation free gain, which becomes even larger in considering the escape of the water molecules into aqueous solution (see above). Therefore, freeing both carboxylate oxygen atoms so that they could bind bidentately to the metal could facilitate the $Ca^{2+} \rightarrow La^{3+}$ exchange in buried and solvent-exposed sites.

La^{3+} as a Substitute for Mg^{2+} in *Mononuclear* Binding Sites. We next studied the $Mg^{2+} \rightarrow La^{3+}$ exchange in mononuclear Mg^{2+}-binding sites containing different combinations of formates and formamide ligands. In analogy with the $Ca^{2+} \rightarrow La^{3+}$ exchange (see above), two types of binding sites in the holoprotein were considered: rigid binding sites that force La^{3+} to adopt the same CN as Mg^{2+} of six:

$$[Mg\,W_{6-m-n}(HCONH_2)_m(HCOO)_n]^{2-n} + [La\,W_9]^{3+} \rightarrow [La\,W_{6-m-n}(HCONH_2)_m(HCOO)_n]^{3-n} + [Mg\,W_6]^{2+} + 3H_2O \quad m = 0, 1;\ n = 1, 2, 3, 4 \quad (4a)$$

and flexible binding sites that allow La^{3+} to expand the CN from six to eight:

$$[Mg\,W_{6-n}(HCOO)_n]^{2-n} + [La\,W_9]^{3+} \rightarrow [La\,W_{8-n}(HCOO)_n]^{3-n} + [Mg\,W_6]^{2+} + H_2O \quad n = 1, 2, 3, 4 \quad (4b)$$

The $Mg^{2+} \rightarrow La^{3+}$ ΔG^x ($x = 1$, 4, 10, 20, and 80) values for eq 4 are listed in Table 5, while some representative structures of the Mg^{2+} and La^{3+} complexes studied are illustrated in Figures 3 and 4, respectively.

The Mg^{2+}−formate complexes possess distorted octahedral symmetry, but upon $Mg^{2+} \rightarrow La^{3+}$ substitution, the complex undergoes significant structural changes so that the shape becomes irregular (compare, for example, Figures 3a and 4a). The $Mg-O^{HCOO}$ bond distances (2.03−2.09 Å, Figure 3) are shorter than the respective $La-O^{HCOO}$ values (2.32−2.46 Å, Figure 4) by roughly 0.3 Å, which is 1 order of magnitude greater than the respective change (∼0.03 Å) upon $Ca^{2+} \rightarrow La^{3+}$ substitution (see Figures 1 and 2). The observed difference is consistent with the fact that for six-coordinated ions, the ionic radius of La^{3+} is significantly larger than that of Mg^{2+} (by 0.31 Å), but it is only slightly larger than that of Ca^{2+} (by 0.03 Å; see Introduction). Thus, the $Mg^{2+} \rightarrow La^{3+}$ exchange results in a more drastic rearrangement of the original metal-binding site than the corresponding $Ca^{2+} \rightarrow La^{3+}$ substitution (see above).

Similarities between $Mg^{2+} \rightarrow La^{3+}$ and $Ca^{2+} \rightarrow La^{3+}$ Exchange. Generally, the trends in ΔG^x for the $Mg^{2+} \rightarrow La^{3+}$ substitution (Table 5) follow those found for the $Ca^{2+} \rightarrow La^{3+}$ exchange (Table 3). In the gas phase and in buried protein cavities, increasing the number of carboxylates helps La^{3+} to replace Mg^{2+} (Table 3, ΔG^x values, $x \leq 10$, in going from reaction 1 → 4 become more negative). Furthermore, in relatively buried bulky complexes containing three or four carboxylates, the presence of a Mg-bound formamide facilitates the $Mg^{2+} \rightarrow La^{3+}$ exchange (Table 5, ΔG^x values, $x \leq 10$, for reactions 7 and 8 are more negative than those for reactions 3 and 4, respectively), whereas expanding the CN of La^{3+} from six to eight does *not* facilitate the $Mg^{2+} \rightarrow La^{3+}$ substitution (Table 5, ΔG^x values, $x \leq 10$, for reactions 11 and 12 are less negative and more positive than those for reactions 3 and 4, respectively).

Differences between $Mg^{2+} \rightarrow La^{3+}$ and $Ca^{2+} \rightarrow La^{3+}$ Exchange. The $Mg^{2+} \rightarrow La^{3+}$ and $Ca^{2+} \rightarrow La^{3+}$ substitutions

Table 5. Calculated ΔG^x (kcal/mol) for $Mg^{2+} \rightarrow La^{3+}$ Exchange in Six-Coordinated Mononuclear Mg Complexes in Media of Dielectric Constant, x

reaction no.	reactant metal complex + $[La\ W_9]^{3+}$	product metal complex + $[Mg\ W_6]^{2+}$	$\Delta\Delta q^a$	$\Delta H^{1,b}$	$T\Delta S^{1,b}$	$\Delta G^{1,b}$	ΔG^4	ΔG^{10}	ΔG^{20}	$\Delta G^{80,c}$
	Rigid Sites, $CN^{Mg} = 6$; $CN^{La} = 6$									
1	$[Mg\ W_5(HCOO)]^+$	$[LaW_5(HCOO)]^{2+} + 3W$	0.04	1.6	25.3	−23.7	9.4	14.8	16.3	20.3
2	$[Mg\ W_4(HCOO)_2]^0$	$[LaW_4(HCOO)_2]^+ + 3W$	0.03	−86.3	26.7	−113.0	−7.5	13.4	20.5	28.9
3	$[Mg\ W_3(HCOO)_3]^-$	$[LaW_3(HCOO)_3]^0 + 3W$	0.05	−176.6	27.7	−204.3	−33.2	1.0	12.4	24.0
4	$[Mg\ W_2(HCOO)_4]^{-2}$	$[LaW_2(HCOO)_4]^- + 3W$	0.05	−267.0	26.5	−293.5	−55.0	−5.0	11.9	28.0
5	$[Mg\ W_4\ Fm(HCOO)]^+$	$[La\ W_4\ Fm(HCOO)]^{2+} + 3W$	0.03	−13.8	26.7	−40.5	8.7	17.9	20.6	25.5
6	$[Mg\ W_3\ Fm(HCOO)_2]^0$	$[La\ W_3\ Fm(HCOO)_2]^+ + 3W$	0.04	−97.8	26.3	−124.1	−10.8	12.6	20.5	29.7
7	$[Mg\ W_2\ Fm(HCOO)_3]^-$	$[La\ W_2\ Fm(HCOO)_3]^0 + 3W$	0.07	−183.7	27.0	−210.7	−40.4	−5.6	6.0	17.9
8	$[Mg\ W_1\ Fm(HCOO)_4]^{-2}$	$[La\ W_1\ Fm(HCOO)_4]^- + 3W$	0.05	−267.2	27.5	−294.7	−60.1	−10.6	6.3	22.5
	Flexible Sites, $CN^{Mg} = 6$; $CN^{La} = 8$									
9	$[Mg\ W_5(HCOO)]^+$	$[LaW_7(HCOO)]^{2+} + W$	0.05	−43.4	4.3	−47.7	4.6	15.9	19.7	23.9
10	$[Mg\ W_4(HCOO)_2]^0$	$[LaW_6(HCOO)_2]^+ + W$	0.04	−121.0	6.5	−127.5	−12.3	12.1	20.7	28.6
11	$[Mg\ W_3(HCOO)_3]^-$	$[LaW_5(HCOO)_3]^0 + W$	0.08	−198.5	5.6	−204.1	−24.5	13.1	26.1	37.4
12	$[Mg\ W_2(HCOO)_4]^{-2}$	$[LaW_4(HCOO)_4]^- + W$	0.08	−278.0	3.7	−281.7	−37.5	14.5	32.6	47.8

[a] $\Delta\Delta q = \Delta q_{La} - \Delta q_{Mg} = (3 - q_{La}) - (2 - q_{Mg})$. [b] Computed at the B3-LYP/(SDD, 6-31+G*)//S-VWN/(SDD, 6-31+G*) level. [c] Computed using the *experimental* hydration free energy of water (−6.3 kcal/mol[59]).

do, however, differ in the magnitudes of the exchange free energies. In the gas phase, the $Mg^{2+} \rightarrow La^{3+}$ exchange is less favorable than the respective $Ca^{2+} \rightarrow La^{3+}$ substitution (the ΔG^1 values in Table 5 are less negative than those in Table 3). This may be mainly attributed to the difference between the charge-accepting abilities of Mg^{2+} vs Ca^{2+}. Calcium is a poorer charge acceptor than Mg^{2+} (compare $\Delta\Delta q$ of 0.16−0.20e in Table 3 with $\Delta\Delta q$ of 0.03−0.08e in Table 5), resulting in weaker electrostatic interactions in Ca^{2+} complexes, as compared to those in Mg^{2+} complexes. On the other hand, La^{3+} is a better charge acceptor than Ca^{2+} or Mg^{2+}; thus it has the strongest metal−ligand interactions. Consequently, the free energy gain upon La^{3+} substitution is larger for Ca^{2+} complexes than that for the respective Mg^{2+} complexes.

In buried and solvent-exposed metal-binding sites, the $Mg^{2+} \rightarrow La^{3+}$ exchange is also less favorable than the respective $Ca^{2+} \rightarrow La^{3+}$ substitution (the ΔG^x values, $x \geq 4$, in Table 5 are less negative and more positive than those in Table 3). Solvation effects do not reverse the gas-phase free energy trend mainly because the hexacoordinated $[Mg\ W_6]^{2+}$ and $[Ca\ W_6]^{2+}$ complexes have similar solvation free energies: $\Delta G^x(Mg\ W_6) - \Delta G^x(Ca\ W_6) = -1.8, -1.4, -0.9$, and -0.5 kcal/mol for $x = 4$, 10, 20, and 80, respectively. The hexacoordinated $[Mg\ W_6]^{2+}$ and $[Ca\ W_6]^{2+}$ complexes also have similar solvation free energy gain upon escaping from the protein cavity (characterized by $x = 4$, 10, or 20) into solution ($x = 80$): the $\Delta G^{80}(Mg\ W_6) - \Delta G^x(Mg\ W_6) = -55.9, -22.2$, and -10.0 kcal/mol, while $\Delta G^{80}(Ca\ W_6) - \Delta G^x(Ca\ W_6) = -57.2, -23.1$, and -10.4 kcal/mol for $x = 4$, 10, and 20, respectively. In *fully solvent-exposed* sites, La^{3+} cannot replace Mg^{2+} (positive ΔG^{80} values for all reactions in Table 5), but it could replace Ca^{2+} if the metal is bound bidentately to only one carboxylate group (negative ΔG^{80} for reaction 1 in Table 3).

La^{3+} as a Substitute for Mg^{2+} in *Binuclear* Binding Sites. Binuclear metal binding sites are found in several metalloproteins where they participate in catalytic processes. Therefore, it is of particular interest to examine the $Mg^{2+} \rightarrow La^{3+}$ substitution in binuclear Mg^{2+}-binding sites, which are modeled to contain two hexacoordinated metal cations connected via a formate bridge (•HCOO•), as shown in Figures 5 and 6.

The first $Mg^{2+} \rightarrow La^{3+}$ exchange was modeled as:

$$[Mg\ W_{5-n}(HCOO)_n \bullet \underline{HCOO} \bullet Mg\ W_{5-m}(HCOO)_m]^{3-n-m} + [La\ W_9]^{3+} \rightarrow [La\ W_{5-n}(HCOO)_n \bullet \underline{HCOO} \bullet Mg\ W_{5-m}(HCOO)_m]^{4-n-m} + [Mg\ W_6]^{2+} + 3H_2O \quad m = 0, 1;\ n = 0-3 \quad (5a)$$

while the second $Mg^{2+} \rightarrow La^{3+}$ exchange was modeled as:

$$[La\ W_2(HCOO)_3 \bullet \underline{HCOO} \bullet Mg\ W_{5-m}(HCOO)_m]^{1-m} + [La\ W_9]^{3+} \rightarrow [La\ W_2(HCOO)_3 \bullet \underline{HCOO} \bullet La\ W_{5-m}(HCOO)_m]^{2-m} + [Mg\ W_6]^{2+} + 3H_2O \quad m = 0, 1 \quad (5b)$$

Generally, the trends in ΔG^x for the $Mg^{2+} \rightarrow La^{3+}$ substitution in a binuclear Mg^{2+}-binding site (Table 6) follow those found for the respective substitution in a mononuclear Mg^{2+}-binding site (Table 5). In fully solvent-exposed *bi*nuclear binding sites, La^{3+} cannot replace Mg^{2+} (Table 6, positive ΔG^{80}) because the solvation free energy gain of the dicationic $[Mg\ W_6]^{2+}$ product cannot compensate for the desolvation cost of the tricationic $[La\ W_9]^{3+}$ reactant. In deeply buried *bi*nuclear Mg^{2+}-binding cavities, the first $Mg^{2+} \rightarrow La^{3+}$ substitution is facilitated by (i) increasing the number of carboxylates (Table 6, ΔG^4 values in going from reaction 1 → 5 become more negative) and (ii) reducing the net positive charge of the second Mg^{2+}-binding site by binding a formate to the second Mg^{2+} (Table 6, ΔG^4 for reaction 5 is more negative than that for reaction 4).

Differences between First and Second $Mg^{2+} \rightarrow La^{3+}$ Substitution. In deeply buried *bi*nuclear sites containing a given number of carboxylates, the second $Mg^{2+} \rightarrow La^{3+}$ substitution appears thermodynamically less favorable than the first one (Table 6, ΔG^4 values for the last two reactions are more positive and less negative than ΔG^4 values for reactions 4 and 5, respectively). Hence, although La^{3+} can replace the first Mg^{2+} in such *bi*nuclear sites, it may not be able to replace the second Mg^{2+} unless another carboxylate is introduced in the metal-

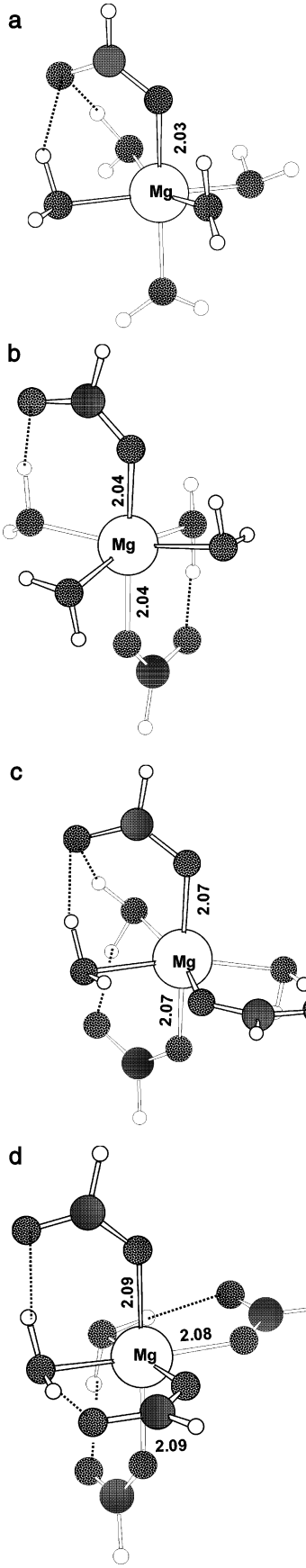

Figure 3. Ball-and-stick diagram of the fully optimized hexa-coordinated (a) $[Mg\ W_5\ (HCOO)]^{+}$, (b) $[Mg\ W_4\ (HCOO)_2]^{0}$, (c) $[Mg\ W_3\ (HCOO)_3]^{-}$, and (d) $[Mg\ W_2\ (HCOO)_4]^{-2}$.

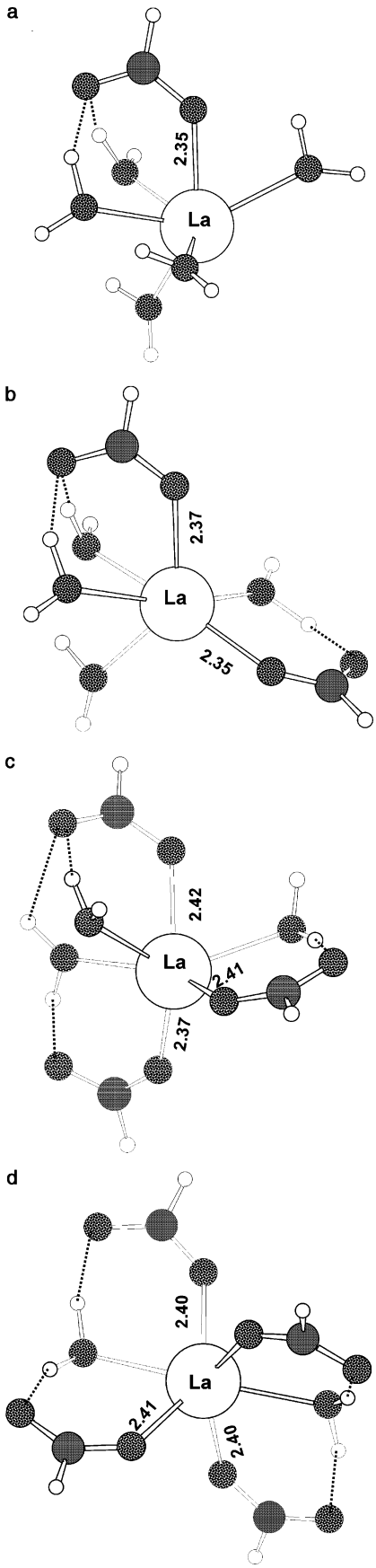

Figure 4. Ball-and-stick diagram of the fully optimized hexa-coordinated (a) $[La\ W_5\ (HCOO)]^{2+}$, (b) $[La\ W_4\ (HCOO)_2]^{+}$, (c) $[La\ W_3\ (HCOO)_3]^{0}$, and (d) $[La\ W_2\ (HCOO)_4]^{-}$.

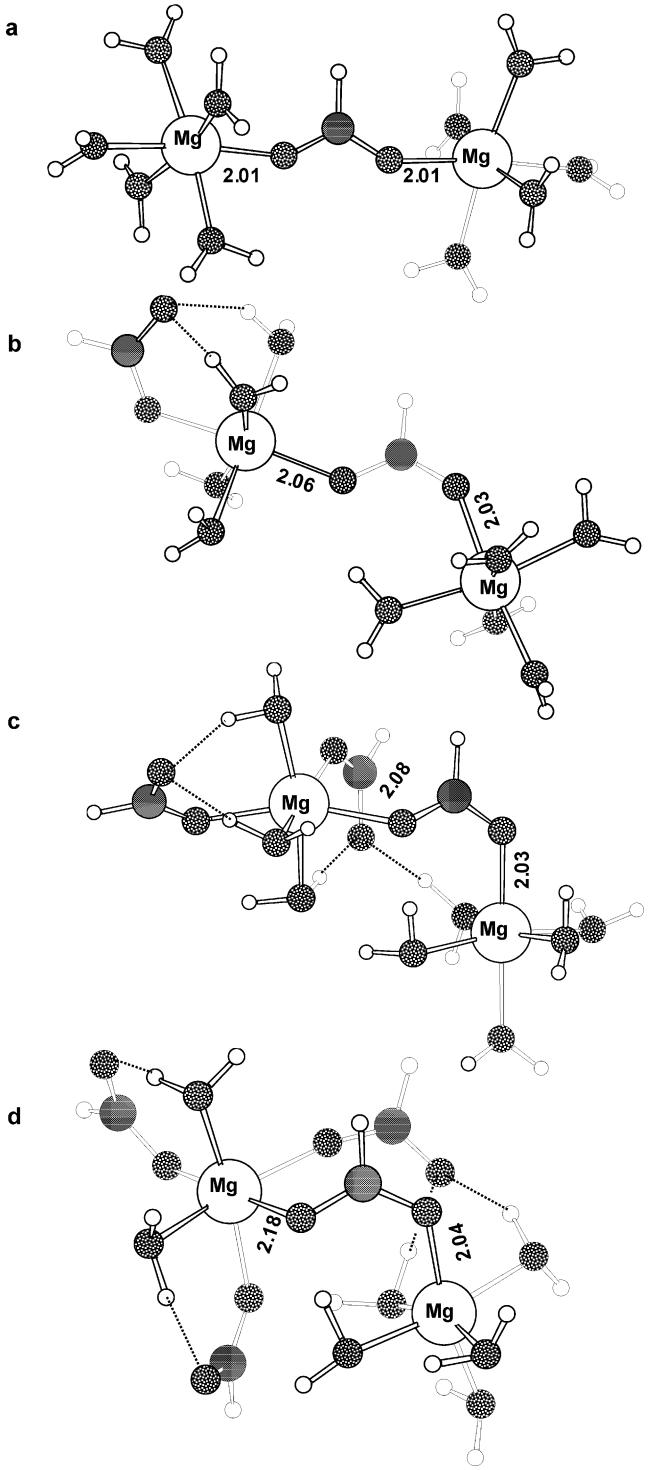

Figure 5. Ball-and-stick diagram of the fully optimized binuclear (a) [**Mg** W_5 •HCOO• Mg W_5]$^{3+}$, (b) [**Mg** W_4 HCOO •HCOO• Mg W_5]$^{2+}$, (c) [**Mg** W_3 $(HCOO)_2$ •HCOO• Mg W_5]$^{+}$, and (d) [**Mg** W_2 $(HCOO)_3$ •HCOO• Mg W_5]^{0}.

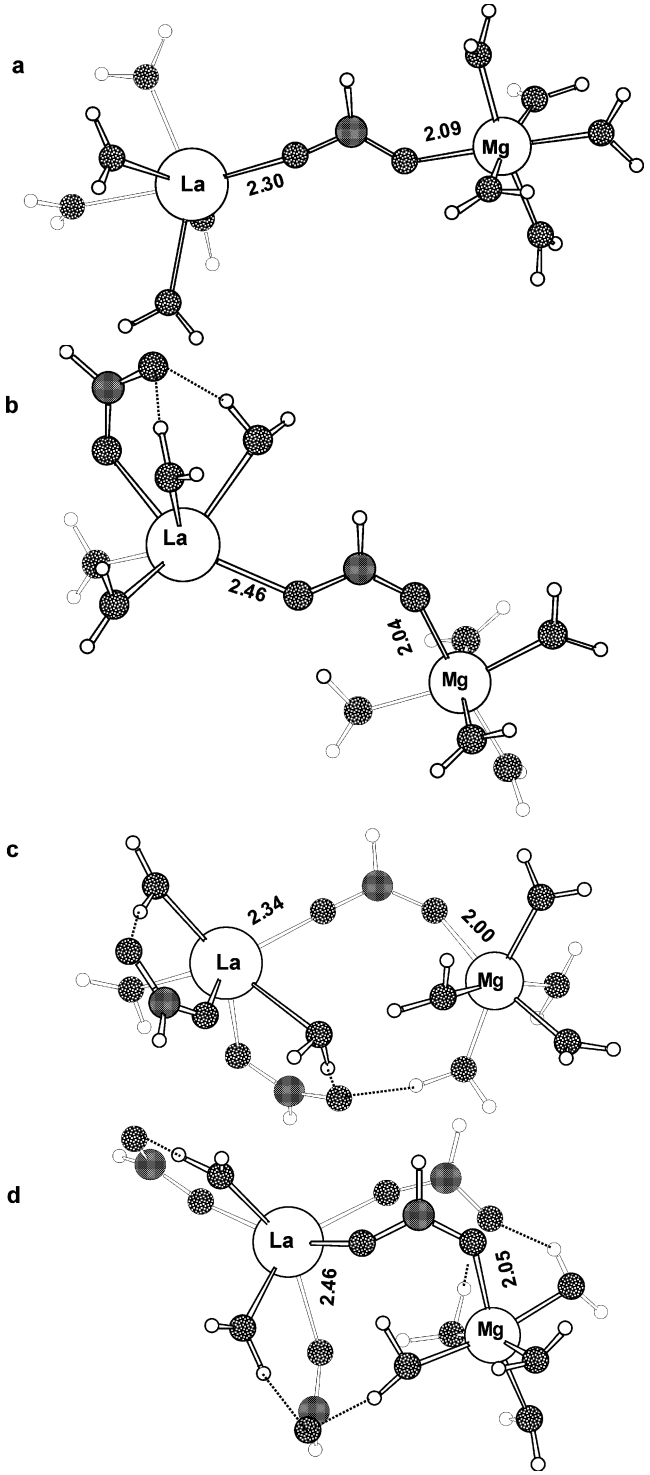

Figure 6. Ball-and-stick diagram of the fully optimized binuclear (a) [**La** W_5 •HCOO• Mg W_5]$^{4+}$, (b) [**La** W_4 HCOO •HCOO• Mg W_5]$^{3+}$, (c) [**La** W_3 $(HCOO)_2$ •HCOO• Mg W_5]$^{2+}$, and (d) [**La** W_2 $(HCOO)_3$ •HCOO• Mg W_5]$^{+}$.

exchange site to bind the second La^{3+} (Table 6, ΔG^4 is positive for reaction 6, but is negative for the last reaction).

Differences between $Mg^{2+} \rightarrow La^{3+}$ Substitution in Mononuclear and Binuclear Mg^{2+}-Binding Sites. The ΔG^x values ($x = 1$, 4, 10, 20, and 80) for *bi*nuclear Mg^{2+}-binding sites show interesting differences from the respective ΔG^x for *mono*nuclear sites. As compared to the *mono*nuclear Mg^{2+}-binding sites containing the same number of carboxylates, the first $Mg^{2+} \rightarrow La^{3+}$ substitution is *less* favorable in deeply buried or partially buried *bi*nuclear sites: the ΔG^x values, $x \leq 10$, for reactions 1−4 in Table 6 are less negative and more positive than the respective numbers for reactions 1−4 in Table 5. This is probably because the net positive charge of the second Mg^{2+}-binding site hinders the $Mg^{2+} \rightarrow La^{3+}$ substitution. Conse-

Table 6. Calculated ΔG^x (kcal/mol) for $Mg^{2+} \rightarrow La^{3+}$ Exchange in Binuclear Mg Complexes in Media of Dielectric Constant, x

reaction no.	reactant metal complex + $[La\ W_9]^{3+}$	product metal complex + $[Mg\ W_6]^{2+}$ + 3W	$\Delta H^{1,a}$	$T\Delta S^{1,a}$	$\Delta G^{1,a}$	ΔG^4	ΔG^{10}	ΔG^{20}	$\Delta G^{80,c}$
	First $Mg^{2+} \rightarrow La^{3+}$ Substitution								
1	[**Mg** W_5•HCOO•Mg W_5]$^{3+}$	[**La** W_5•HCOO•Mg W_5]$^{4+}$	94.8	27.1	67.7	27.7	18.2	14.5	14.5
2	[**Mg** W_4 HCOO•HCOO•Mg W_5]$^{2+}$	[**La** W_4 HCOO•HCOO•Mg W_5]$^{3+}$	31.4	27.5	3.9	18.3	19.7	19.8	22.4
3	[**Mg** W_3 $(HCOO)_2$•HCOO•Mg W_5]$^{+}$	[**La** W_3 $(HCOO)_2$•HCOO•Mg W_5]$^{2+}$	−42.5	29.0	−71.5	−6.0	7.6	12.1	18.8
4	[**Mg** W_2 $(HCOO)_3$•HCOO•Mg W_5]^{0}	[**La** W_2 $(HCOO)_3$•HCOO•Mg W_5]$^{+}$	−113.6	28.2	−141.8	−25.0	−0.6	7.7	17.2
5	[**Mg** W_2 $(HCOO)_3$•HCOO•Mg W_4 HCOO]$^{-}$	[**La** W_2 $(HCOO)_3$•HCOO•Mg W_4 HCOO]^{0}	−169.0	27.5	−196.5	−29.3	4.7	16.1	27.8
	Second $Mg^{2+} \rightarrow La^{3+}$ Substitution								
6	[La W_2 $(HCOO)_3$•HCOO•**Mg** W_5]$^{+}$	[La W_2 $(HCOO)_3$•HCOO•**La** W_5]$^{2+}$	−14.3	26.2	−40.5	11.6	20.5	23.1	28.0
7	[La W_2 $(HCOO)_3$•HCOO•**Mg** W_4 HCOO]^{0}	[La W_2 $(HCOO)_3$•HCOO•**La** W_4 HCOO]$^{+}$	−110.4	27.9	−138.2	−24.5	−1.3	6.5	15.6

[a] Computed at the B3-LYP/(SDD, 6-31+G*)//S-VWN/(SDD, 6-31+G*) level. [c] Computed using the *experimental* hydration free energy of water (−6.3 kcal/mol[59]).

Table 7. Experimental and Computed Average Metal−O($HCOO^-$) Distances in Seven-Coordinated La/Ca and Six-Coordinated La/Mg Complexes

metal–O(COO^-)	calcd (Å)	expt (Å)
Seven-Coordinated La/Ca Complexes		
⟨La−O⟩	2.44[a]	2.46[d]
⟨La−$\tilde{O}$⟩	2.50[b]	2.58[d]
⟨La−$\tilde{O}_1$⟩ − ⟨La−$\tilde{O}_2$⟩	0.02[c]	0.05[d]
⟨Ca−O⟩	2.41[a]	2.37[e]
⟨Ca−$\tilde{O}$⟩	2.47[b]	2.53[e]
⟨Ca−$\tilde{O}_1$⟩ − ⟨Ca−$\tilde{O}_2$⟩	0.06[c]	0.11[e]
Six-Coordinated Ln/Mg Complexes		
⟨La−O⟩/⟨Gd−O⟩	2.40[f]	2.31[g]
⟨Mg−O⟩	2.06[f]	2.13[h]

[a] Average M−O($HCOO^-$) (M = La or Ca) in four monodentate complexes: $[M\ W_5\ Fm\ (HCOO)]^{2+/+}$, $[M\ W_4\ Fm\ (HCOO)_2]^{+/0}$, $[M\ W_3\ Fm\ (HCOO)_3]^{0/-}$, $[M\ W_2\ Fm\ (HCOO)_4]^{-/2-}$. [b] Average M−$\tilde{O}$($H\tilde{C}OO^-$) (M = La or Ca) in three bidentate complexes: $[M\ W_4\ Fm\ (H\tilde{C}O\tilde{O})_2]^{+/0}$, $[M\ W_2\ Fm\ (H\tilde{C}O\tilde{O})_2]^{+/0}$, $[M\ Fm\ (H\tilde{C}O\tilde{O})_3]^{0/-}$. [c] The difference between the two M−$\tilde{O}$ distances in $[M\ W_4\ Fm\ (H\tilde{C}O\tilde{O})]^{2+/+}$ (M = La or Ca) complexes. [d] Average La−O/$\tilde{O}$($HCOO^-$) from a 2.60 Å X-ray structure of a EF-hand binding site in which Ca^{2+} has been replaced with La^{3+}. [e] Average Ca−O/$\tilde{O}$(Asp) from Ca-binding sites in the PDB, in which Ca is heptacoordinated.[40] [f] Average M−O($HCOO^-$) (M = La or Mg) in eight monodentate complexes: $[M\ W_5\ (HCOO)]^{2+/+}$, $[M\ W_4\ (HCOO)_2]^{+/0}$, $[M\ W_3\ (HCOO)_3]^{0/-}$, $[M\ W_2\ (HCOO)_4]^{-/2-}$, $[M\ W_4\ Fm\ (HCOO)]^{2+/+}$, $[M\ W_3\ Fm\ (HCOO)_2]^{+/0}$, $[M\ W_2\ Fm\ (HCOO)_3]^{0/-}$, $[M\ W\ Fm\ (HCOO)_4]^{-/2-}$. [g] Average Gd−O(HCOO) from two PDB structures of inositol monophosphatase (PDB entries 1IMA and 1IMB). Note that La−O bond distances are expected to be longer than Gd−O bond distances because of the larger ionic radius of La^{3+} (1.17 Å) compared to that of Gd^{3+} (1.08 Å). [h] Average Mg−O from Mg-binding sites in the PDB.[40]

quently, in proteins containing *mono*nuclear and *bi*nuclear Mg^{2+}-binding sites, the $Mg^{2+} \rightarrow La^{3+}$ substitution would occur more readily in the former than in the latter.

Discussion

Comparison with PDB Structures. The average metal−O($HCOO^-$) distances in the fully optimized seven-coordinated La/Ca and six-coordinated La/Mg complexes show trends similar to those found in the respective metal-binding sites in the PDB, as shown in Table 7. The average metal−O(monodentate) distances are shorter than the metal−$\tilde{O}$(bidentate) ones. For a given metal CN, the La−O/$\tilde{O}$ distances are longer than the respective Ca−O/$\tilde{O}$ or Mg−O distances, in line with the larger ionic radius of La^{3+} compared with that of Ca^{2+} and Mg^{2+} (see Introduction). Interestingly, both experiments and our calculations show that the difference between the two Ca−$\tilde{O}$(bidentate) distances (0.06−0.11 Å) is on average greater than that between the two La−$\tilde{O}$(bidentate) distances (0.02−0.05 Å).

The preferred La^{3+} CN is in accord with that found in PDB structures containing lanthanide cations. In replacing Ca^{2+} bound to different numbers of formates in various binding modes, La^{3+} prefers a CN of seven rather than eight (Table 3, ΔG^x values, $x \geq 4$, for reactions 1−4 are more negative and less positive than the corresponding ΔG^x values for reactions 9−12). These results are consistent with the finding that octacoordinated lanthanides are not found in EF-hand binding sites and they are less common than the heptacoordinated metal in lanthanide-binding sites. In analogy to the $Ca^{2+} \rightarrow La^{3+}$ substitution, upon replacing Mg^{2+} bound to three and four formates in the respective buried sites, La^{3+} generally prefers to adopt the CN of the native metal (six for Mg^{2+}) rather than expanding the CN to eight (Table 5, ΔG^4 values for reactions 3 and 4 are more negative than the corresponding ΔG^x values for reactions 11 and 12, respectively. This is consistent with the observation that lanthanide cations (Gd^{3+}) adopt a six-coordinated geometry upon binding to a binuclear Mg-binding site in inositol monophosphatase.[18]

For a given EF-hand-like binding site, La^{3+} prefers to bind to at least one carboxylate bidentately rather than monodentately (Table 4, ΔG^x values, $x \geq 4$, for reactions 2−4 and 6−9 are more negative and less positive than those for reactions 1 and 5, respectively). This is in line with the finding that all EF-hand-like La-binding sites in the PDB contain at least one bidentately bound Asp/Glu. Furthermore, a lanthanide Eu^{3+} cation that was introduced to a binuclear Mg^{2+}-binding site in the Klenow fragment of DNA polymerase I binds to the bridging aspartate bidentately rather than monodentately, thus disrupting the active site and abolishing the catalytic activity of the enzyme.[22] Note, however, that the computed free energy difference between the bidentate structure and the respective monodentate structure is an upper bound because the metal-free carboxylate oxygen in the monodentate structure could be stabilized by interactions with non-first-shell ligands, which have been neglected in the present calculations. Indeed, in one protein, cyclodextrin glucanotransferase (PDB entry 1PAM), all the acidic residues in the two Ca-binding sites are monodentately bound, as the metal-free carboxylate oxygen atoms are stabilized by hydrogen-bonding interactions with second-shell water molecules.

Factors Favoring the Substitution of La^{3+} for Ca^{2+}/Mg^{2+} in Holoproteins. Whether La^{3+} can replace Ca^{2+}/Mg^{2+} in the respective metal-binding site in a holoprotein depends on several factors. These include (1) the solvent exposure of the metal-

binding site, (2) the flexibility of the metal-binding site, (3) the number of carboxylate *oxygen atoms* available for binding bidentately to La^{3+}, (4) the number of metal-bound carboxylate groups, (5) the absence or presence of a backbone or side chain metal-bound carbonyl group, and (6) the nature of the exchanging metal (Ca^{2+}/Mg^{2+}; mononuclear vs binuclear).

(1) Dependence on the Metal-Binding Site's Solvent Exposure. A solvent-shielded Ca^{2+}/Mg^{2+}-binding cavity facilitates La^{3+} to replace Ca^{2+}/Mg^{2+}, as evidenced by the negative ΔG^1 but generally positive ΔG^{80} values in Tables 3−5. The latter is mainly because in solvent-exposed sites, the desolvation cost of the incoming trivalent La^{3+} cation exceeds the solvation free energy gain of the displaced divalent Ca^{2+}/Mg^{2+} cation. Furthermore, the desolvation cost of a negatively charged Ca^{2+}/Mg^{2+} complex of net charge $-Q$ is greater than the solvation free energy gain of the respective La-substituted complex with a smaller net charge of $-Q + 1$ (see Scheme 1). Indeed, in fully solvent-exposed Mg-binding sites, La^{3+} is predicted not to displace Mg^{2+} (Table 5, positive ΔG^{80}).

(2) Dependence on the Metal-Binding Site's Flexibility. A rigid, as opposed to a flexible, Ca^{2+}/Mg^{2+}-binding site generally facilitates La^{3+} to replace Ca^{2+}/Mg^{2+}: the ΔG^x values, $x > 4$, in Tables 3−5 are more negative and less positive in rigid sites that force La^{3+} to retain the native CN than in flexible sites that allow La^{3+} to expand its CN. This is mainly because the heptacoordinated La complexes in rigid sites are better solvated than the respective bulkier octacoordinated La complexes in flexible sites; furthermore, more water molecules are released in rigid sites, as compared to flexible sites. These factors result in a gain in both the gas-phase entropy and in the solvation free energy of the released water molecules.

(3) Dependence on the Carboxylate-Binding Mode. For a given metal−carboxylate complex, freeing both carboxylate oxygen atoms so that they could bind bidentately to La^{3+} facilitates it to replace Ca^{2+}/Mg^{2+}: the ΔG^x values, $x \geq 4$, for reactions 2−4 or 6−9 in Table 4 are more negative than those for reaction 1 or 5, respectively. This is because as more carboxylates become bidentately (rather than monodentately) bound to La^{3+}, more metal-bound water molecules are released, resulting in a gain in both the gas-phase entropy and in the solvation free energy of the released water molecules.

(4) Dependence on the Number of Metal-Bound Carboxylate Groups. The presence of Asp/Glu side chains has opposite effects on the ease of $Ca^{2+}/Mg^{2+} \rightarrow La^{3+}$ exchange depending on the solvent accessibility of the metal-binding site. In *buried* sites, increasing the number of negatively charged Asp/Glu that can bind the metal facilitates the $Ca^{2+}/Mg^{2+} \rightarrow La^{3+}$ exchange: the ΔG^x values, $x \leq 10$, in Tables 3 and 5 become more negative in going from reaction 1 → 4. This is mainly because trivalent La^{3+} can accept more negative charge from the carboxylate side chains than divalent Ca^{2+}/Mg^{2+} (Tables 3 and 5, positive $\Delta\Delta q$). In *solvent-exposed* sites, however, minimizing the number of metal-bound Asp/Glu residues helps La^{3+} to replace Ca^{2+}: in Table 3, the ΔG^x values, $x > 10$, become more negative in going from reaction 4 → 1. This is because with only one carboxylate group bound to the metal, the desolvation cost of the *monocationic* Ca^{2+} complex is outweighed by the solvation free energy gain of the respective *dicationic* La-substituted complex. Note, however, that in solvent-exposed sites, even if only one Asp/Glu side chain is bound to Mg^{2+}, La^{3+} cannot displace Mg^{2+} (Table 5, positive ΔG^{80}; see also above).

(5) Dependence on the Absence or Presence of a Backbone or Side Chain Metal-Bound Carbonyl Group. The presence of the peptide backbone or a Asn/Gln side chain has opposite effects on the ease of $Ca^{2+}/Mg^{2+} \rightarrow La^{3+}$ exchange depending on the number of metal-bound carboxylates. Binding of a carbonyl group from the peptide backbone or the Asn/Gln side chain to the metal would prohibit the $Ca^{2+} \rightarrow La^{3+}$ exchange in complexes containing only one Asp/Glu residue, especially if the site is not deeply buried: in Table 3, the ΔG^x values, $x \geq 4$, for reaction 5 are less negative than those for reaction 1. This is because unfavorable solvation effects are greater in complexes with a single carboxylate and a carbonyl group than the respective complexes without the carbonyl group (see Results). Binding of a carbonyl group from the peptide backbone or the Asn/Gln side chain to the metal, however, facilitates the $Ca^{2+}/Mg^{2+} \rightarrow La^{3+}$ exchange in bulky complexes with four Asp/Glu residues: in Tables 3 and 5, the ΔG^x values, $x \geq 4$, for reaction 8 are more negative and less positive than those for reaction 4. This may be because the larger La^{3+} can better accommodate steric crowding among the five ligands than the smaller Ca^{2+}/Mg^{2+}.

(6) Dependence on the Nature of the Exchanging Metal. It is easier to substitute the native metal with La^{3+} in Ca^{2+}-binding sites than in the respective Mg^{2+}-binding sites: The $Ca^{2+} \rightarrow La^{3+}$ substitution is accompanied by more favorable exchange free energies than the corresponding $Mg^{2+} \rightarrow La^{3+}$ substitution (compare ΔG^x, $x \geq 4$, in Tables 3 and 5) mainly because electrostatic interactions in Ca^{2+} complexes are weaker than those in Mg^{2+} complexes ($\Delta\Delta q$ values in Table 3 are greater than those in Table 5). Furthermore, less drastic structural rearrangement occurs upon $Ca^{2+} \rightarrow La^{3+}$ exchange, as compared to the corresponding $Mg^{2+} \rightarrow La^{3+}$ substitution (see Figures 1−4).

In buried, binuclear Mg^{2+}-binding sites, the presence of a second Mg^{2+}-binding site with a net positive charge hampers the $Mg^{2+} \rightarrow La^{3+}$substitution ($\Delta G^x$ values, $x \geq 4$, for reactions 1−4 in Table 6 are more positive and less negative than those in Table 5). Thus, in such binuclear sites, maximizing the number of carboxylate groups that can coordinate to La^{3+} facilitates it to replace one or two Mg^{2+}.

Experimental Support. Available experimental data (X-ray, NMR, and thermodynamics) are consistent with the theoretical findings, in particular, the aforementioned factors as governing the relative affinity of trivalent lanthanides vs divalent Ca^{2+}/Mg^{2+} for a given metal-binding site. The finding that a solvent-shielded Ca^{2+}-binding cavity facilitates $Ca^{2+} \rightarrow La^{3+}$ exchange is supported by the experimental finding that in protozoan (*Entamoeba histolytica*) Ca^{2+}-binding protein (EhCaBP), a 134-amino acid monomeric protein containing four canonical EF-hand Ca^{2+}-binding loops, Yb^{3+} displaces Ca^{2+} from the four different metal-binding sites in a sequential manner: first from site III (residues 71−103) and last from site IV (residues 104−134). This is consistent with the fact that site IV is more solvent-exposed than the other sites.[60]

The finding that bidentate carboxylate binding facilitates $Ca^{2+} \rightarrow La^{3+}$ exchange is consistent with the observed switch from

(60) Atreya, H. S.; Mukherjee, S.; Chary, K. V. R.; Lee, Y. M.; Luchinat, C. *Protein Sci.* **2003**, *12*, 412−425.

monodentate to bidentate carboxylate binding when Ca^{2+} is replaced by (a) Yb^{3+} in the EF-hand Ca-binding site of carp parvalbumin[61] and (b) Eu^{3+} in thermolysin.[1]

The finding that increasing the number of metal-bound carboxylate groups in *buried* sites facilitates $Ca^{2+} \rightarrow La^{3+}$ exchange is supported by several experimental findings. (i) The La^{3+} affinity for peptide analogues of the Ca-binding site II of rabbit skeletal troponin C generally increases as more Asp residues are incorporated into the peptide.[62] (ii) In EhCaBP Ca^{2+}-binding protein (see above), Yb^{3+} has the highest binding affinity for the relatively *buried* Ca^{2+}-binding site III, as compared to that of the other sites. This is consistent with the fact that site III has the most number (*four)* of negatively charged Ca^{2+} ligands, whereas the other three sites each has only *three* Asp/Glu coordinated to the metal. (iii) In human MRP8 protein, a member of the S100 EF-hand Ca-binding protein family, replacement with Yb^{3+} occurred *only* in the C-terminal EF-hand site, which has three metal-bound acidic residues, but not in the N-terminal EF-hand site, which has none.[63] (iv) In the *Escherichia coli* galactose chemoreceptor protein, a mutant Ca-binding site with four acidic amino acids exhibits a 10^2-fold preference for lanthanide trications over Ca^{2+}.[64]

The prediction that Ln^{3+} can dislodge Mg^{2+} from a buried *mono*nuclear binding site flanked by at least two carboxylic residues (Table 5) is supported by the finding that the Mg^{2+}-binding site in the chemotaxis protein, CheY, which consists of two aspartates and a backbone carbonyl, shows greater preference toward Ln^{3+} binding (by $\sim 10^3$ times) than the natural cofactor Mg^{2+}.[65] Furthermore, the prediction that La^{3+} can replace one of the Mg^{2+} in a *bi*nuclear binding site containing at least three Asp/Glu residues (Table 6) is supported by the finding that Eu^{3+} has greater (30−50 times) affinity than the natural Mg^{2+} cofactor for site A (consisting of two aspartates and a glutamate) in the *bi*nuclear binding site of the Klenow fragment of *E. coli* polymerase I and bacteriophage T4 DNA polymerase.[20]

In conclusion, the calculations have not only revealed the key factors favoring the substitution of La^{3+} for Ca^{2+} and Mg^{2+} in protein metal-binding sites, but also the physical bases for the governing factors. Some of these factors may not be easy to determine experimentally. For example, it is difficult to distinguish between monodentate and bidentate forms of the lanthanide/calcium/magnesium complexes by NMR.[27] Furthermore, it is difficult to accurately quantify the number of monodentate and bidentate carboxylate ligands bound to lanthanides by fluorescence spectroscopy.[66] In particular, the calculations have revealed some of the factors governing metal selectivity in *binuclear* binding sites, a subject that has been relatively unexplored in previous works.[67] The findings of this study have potential application in engineering a lanthanide-binding site in a protein that does not have such a site.[68,69] They may also be useful in NMR structure determination of Ca^{2+}/Mg^{2+}-binding proteins by suggesting residue substitutions that would enable lanthanide ions to replace the native Ca^{2+}/Mg^{2+} cofactor.

Acknowledgment. We are indebted to Drs. C. Luchinat and M. Akke for stimulating discussion leading to this work. We are grateful to Drs. D. Bashford, M. Sommer, and M. Karplus for the program to solve the Poisson equation. This work was supported by the National Science Council, Taiwan (NSC Contract No. 91-2311-B-001), the Institute of Biomedical Sciences, and the National Center for High-Performance Computing, Taiwan.

JA044404T

(61) Kumar, V. D.; Lee, L.; Edwards, B. F. P. *FEBS Lett.* **1991**, *283*, 311−316.
(62) Marsden, B. J.; Hodges, R. S.; Sykes, B. D. *Biochemistry* **1988**, *27*, 4198−4206.
(63) Ishikawa, K.; Nakagawa, A.; Tanaka, I.; Suzuki, M.; Nishihira, J. *Acta Crystallogr., Sect. D* **2000**, *56*, 559−566.
(64) Falke, J. J.; Snyder, E. E.; Thatcher, K. C.; Voertler, C. S. *Biochemistry* **1991**, *30*, 8690−8697.
(65) Needham, J. V.; Chen, T. Y.; Falke, J. J. *Biochemistry* **1993**, *32*, 3363−3367.
(66) Jegerschold, C.; Rutherford, A. W.; Mattioli, T. A.; Crimi, M.; Bassi, R. *J. Biol. Chem.* **2000**, *275*, 12781−12788.
(67) Dudev, T.; Lim, C. *Chem. Rev.* **2003**, *103*, 773−787.
(68) Clark, I. D.; MacManus, J. P.; Banville, D.; Szabo, A. G. *Anal. Biochem.* **1993**, *210*, 1−6.
(69) MacKenzie, C. R.; Clark, I. D.; Evans, S. V.; Hill, I. E.; MacManus, J. P.; Dubuc, G.; Bundle, D. R.; Narang, S. A.; Young, N. M.; Szabo, A. G. *Immunotechnology* **1995**, *1*, 139−150.